Cell Reports

Article

ADAR1 interaction with Z-RNA promotes editing of endogenous double-stranded RNA and prevents MDA5-dependent immune activation

Graphical abstract

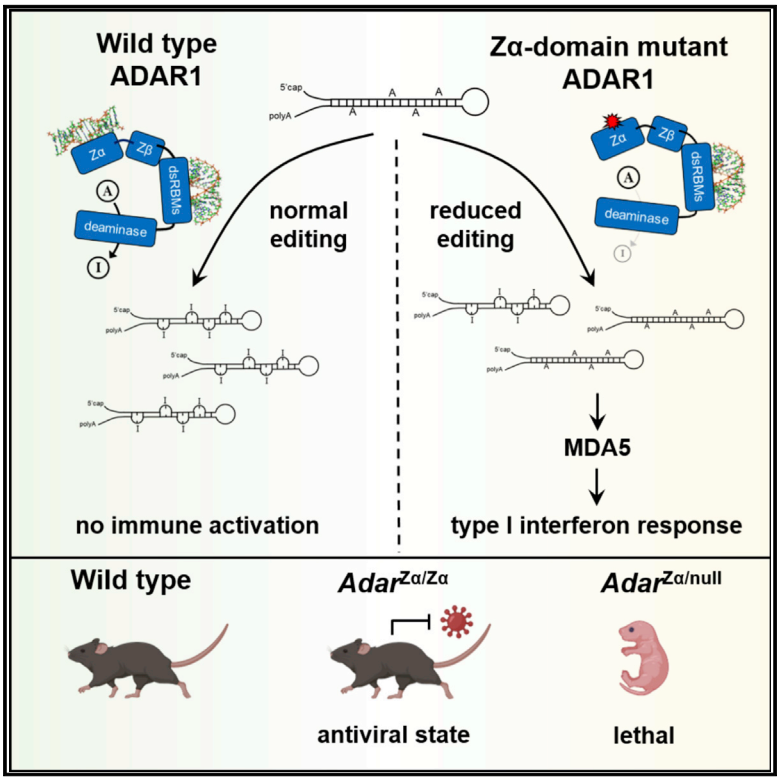

Highlights

- Z-RNA interaction with the Zα domain of ADAR1 promotes editing of self-dsRNA
- Mutation of the Zα domain of ADAR1 triggers an MDA5/MAVS-dependent IFN-I response
- Homozygous ADAR1 Zα domain mutant mice develop a spontaneous IFN-I signature
- Hemizygous expression of Zα domain mutant ADAR1 causes MAVS-dependent lethality

Authors

Richard de Reuver, Evelien Dierick, Bartosz Wiernicki, ..., Filip Van Nieuwerburgh, Peter Vandenabeele, Jonathan Maelfait

Correspondence

jonathan.maelfait@irc.vib-ugent.be

In brief

de Reuver et al. find that interaction of Z-RNA with ADAR1 prevents the development of an MDA5/MAVS-dependent type I interferon response. Mice carrying mutations in ADAR1 that prevent its binding to Z-RNA mimic the severe autoinflammatory phenotype of patients with Aicardi-Goutières syndrome.

de Reuver et al., 2021, Cell Reports *36*, 109500
August 10, 2021
https://doi.org/10.1016/j.celrep.2021.109500

CellPress

Cell Reports

CellPress
OPEN ACCESS

Article

ADAR1 interaction with Z-RNA promotes editing of endogenous double-stranded RNA and prevents MDA5-dependent immune activation

Richard de Reuver,[1,2] Evelien Dierick,[1,2] Bartosz Wiernicki,[1,2] Katrien Staes,[1,2] Leen Seys,[1,3] Ellen De Meester,[3] Tuur Muyldermans,[5] Alexander Botzki,[5] Bart N. Lambrecht,[1,3,6] Filip Van Nieuwerburgh,[4,7] Peter Vandenabeele,[1,2] and Jonathan Maelfait[1,2,8,*]

[1]VIB-UGent Center for Inflammation Research, 9052 Ghent, Belgium
[2]Department of Biomedical Molecular Biology, Ghent University, 9052 Ghent, Belgium
[3]Department of Internal Medicine and Pediatrics, Ghent University, 9000 Ghent, Belgium
[4]NXTGNT, Faculty of Pharmaceutical Sciences, Ghent University, Ottergemsesteenweg 460, 9000 Ghent, Belgium
[5]VIB Bioinformatics Core, VIB, 9052 Ghent, Belgium
[6]Department of Pulmonary Medicine, Erasmus University Medical Center Rotterdam, 3015 GJ Rotterdam, the Netherlands
[7]Laboratory of Pharmaceutical Biotechnology, Faculty of Pharmaceutical Sciences, Ghent University, Ottergemsesteenweg 460, 9000 Ghent, Belgium
[8]Lead contact
*Correspondence: jonathan.maelfait@irc.vib-ugent.be
https://doi.org/10.1016/j.celrep.2021.109500

SUMMARY

Loss of function of adenosine deaminase acting on double-stranded RNA (dsRNA)-1 (ADAR1) causes the severe autoinflammatory disease Aicardi-Goutières syndrome (AGS). ADAR1 converts adenosines into inosines within dsRNA. This process called A-to-I editing masks self-dsRNA from detection by the antiviral dsRNA sensor MDA5. ADAR1 binds to dsRNA in both the canonical A-form and the poorly defined Z conformation (Z-RNA). Mutations in the Z-RNA-binding Zα domain of ADAR1 are common in patients with AGS. How loss of ADAR1/Z-RNA interaction contributes to disease development is unknown. We demonstrate that abrogated binding of ADAR1 to Z-RNA leads to reduced A-to-I editing of dsRNA structures formed by base pairing of inversely oriented short interspersed nuclear elements. Preventing ADAR1 binding to Z-RNA triggers an MDA5/MAVS-mediated type I interferon response and leads to the development of lethal autoinflammation in mice. This shows that the interaction between ADAR1 and Z-RNA restricts sensing of self-dsRNA and prevents AGS development.

INTRODUCTION

Aicardi-Goutières syndrome (AGS) is a severe autoinflammatory disease characterized by chronic type I interferon (IFN-I) production (Rodero and Crow, 2016). AGS results from mutations in one of nine genes including *ADAR*, which codes for adenosine deaminase acting on double-stranded RNA (dsRNA)-1 (ADAR1) (Crow et al., 2015; Rice et al., 2012; Uggenti et al., 2020). ADAR1 converts adenosine (A) residues into inosines (I) within double-stranded dsRNA. This process called A-to-I editing marks endogenous dsRNA as self and masks these molecules from detection by the cytosolic nucleic acid sensor MDA5. Mutations that disrupt the activity of ADAR1, such as in AGS, trigger a deleterious MDA5-mediated IFN-I response.

ADAR1 edits dsRNA structures formed by base pairing of two adjacent and inversely oriented short interspersed nuclear elements (SINEs). These SINEs include the human *Alu* elements and mouse B1 or B2 repeats, which are abundantly present in introns and 3′ untranslated regions (UTRs) of messenger RNAs (mRNAs) (Athanasiadis et al., 2004; Blow et al., 2004; Kim et al., 2004; Levanon et al., 2004; Neeman et al., 2006). A-to-I editing of endogenous SINE-derived duplex RNA thus forms an important barrier to prevent spontaneous MDA5 activation (Ahmad et al., 2018; Chung et al., 2018). This is supported by the analysis of *Adar* knockout or editing-deficient mice, which develop an MDA5/MAVS-mediated IFN-I response (Bajad et al., 2020; Liddicoat et al., 2015; Mannion et al., 2014; Pestal et al., 2015).

ADAR encodes two isoforms: a constitutively expressed short transcript (p110) and a long isoform (p150) that is transcribed from an IFN-inducible promotor. ADAR1 binds to the canonical A conformation of dsRNA (A-RNA) while the larger p150 isoform contains an N-terminal Zα domain, which specifically interacts with nucleic acids that have adopted the unusual Z conformation, including Z-form RNA (Z-RNA) (Placido et al., 2007). Recent evidence shows that both viral and endogenous Z-RNA sequences bind to the tandem Zα domains of the nucleic acid sensor ZBP1. This then triggers ZBP1 activation and contributes

to cell-intrinsic antiviral immunity or, when aberrantly activated, to the development of inflammatory disease (Devos et al., 2020; Jiao et al., 2020; Kesavardhana et al., 2017, 2020; Maelfait et al., 2017; Sridharan et al., 2017; Wang et al., 2020; Zhang et al., 2020). These findings revealed a role for the recognition of Z-RNA by Zα domains of ZBP1 in inducing an immune response. How Z-RNA relates to ADAR1 function and whether the Zα domain in ADAR1 is important for its immunosuppressive effects remain unknown.

Mice that only express ADAR1-p110 and that are deficient for the Zα domain containing p150 isoform phenocopy full *Adar*-deficient animals and develop an MDA5/MAVS-dependent IFN-I response (Pestal et al., 2015; Ward et al., 2011). Interestingly, more than half of *ADAR* patients with AGS contain compound heterozygous mutations with one allele carrying the p.Pro193Ala mutation in the Zα domain of ADAR1-p150 combined with another dysfunctional *ADAR* allele (Rice et al., 2012, 2017). Taken together, this strongly suggests that A-to-I editing by the ADAR1-p150 isoform is the primary mechanism by which MDA5 evades recognition of endogenous dsRNA and that the interaction of ADAR1 with Z-RNA contributes to this inhibitory activity. However, experimental evidence that supports this hypothesis is lacking.

We generated human cell lines and *Adar* knockin mice expressing an ADAR1 protein that is unable to interact with Z-RNA. We found that Z-RNA binding to ADAR1 is required to enable efficient A-to-I editing of duplex RNA formed by oppositely oriented human *Alu* or mouse B1 or B2 SINEs. Mutation of the Zα domain of ADAR1 led to the accumulation of dsRNA and triggered an MDA5-mediated IFN-I response. Homozygous *Adar* Zα domain mutant mice showed mild immune activation and were more resistant to virus infection but did not develop autoinflammatory disease. In contrast, mice that hemizygously express Zα domain mutant ADAR1, thereby mimicking the compound heterozygous state of patients with AGS, developed a lethal MAVS-mediated IFN-I response. We propose that the Zα domain of ADAR1 widens its editing repertoire by interacting with Z-RNA structures in duplex RNA substrates. Binding of ADAR1 to Z-RNA therefore contributes to the discrimination between self and non-self and is important in preventing genetic disease such as AGS.

RESULTS

ADAR1 Zα domain mutation activates MDA5 in human cells

The *ADAR* p.Pro193Ala missense mutation located in the Z-form nucleic acid binding Zα domain of ADAR1 occurs in the compound heterozygous state with a dysfunctional *ADAR* allele in half of *ADAR* AGS cases (Figure 1A) (Rice et al., 2017). Proline 193 is located in the β loop that connects the Z-form nucleic acid recognition α3 helix with two C-terminal antiparallel β2 and β3 sheets in the Zα domain of ADAR1 (Placido et al., 2007; Schwartz et al., 1999). Proline mutations often result in structural irregularities and may cause Zα domain misfolding. To specifically address the impact of disrupted binding of ADAR1 to Z-RNA, we therefore introduced N173A/Y177A amino acid substitutions in the α3 helix of the Zα domain of ADAR1, which fully abrogate binding to Z-form nucleic acids without altering overall Zα domain structure (Feng et al., 2011; Schade et al., 1999). We generated four HEK293 clones with Zα domain mutant *ADAR* ($ADAR^{Z\alpha mut}$) alleles (Figures S1A and S1B). All alleles carried the Y177A mutation; however, we detected at least one intact N173 allele in every clone (Figure S1A), possibly due to incomplete targeting of the hypotriploid HEK293 genome (Bylund et al., 2004). Sole Y177A mutation reduces the affinity of the Zα domain for Z-form nucleic acids by 30-fold (Schade et al., 1999). We reasoned that the remaining Y177A-only protein expressed by this locus would still be compromised in its ability to bind to Z-RNA and would not interfere with the interpretation of our results. As controls, we retained two wild-type ($ADAR^{WT}$) clones and generated an ADAR1-deficient ($ADAR^{KO}$) clone (Figures S1A and S1B). Importantly, Zα domain mutation did not affect ADAR1 p110 or p150 protein expression (Figure S1B).

Loss of ADAR1 in HEK293T cells induced an MDA5-dependent IFN-I response and led to a spontaneous activation of the dsRNA sensor and translational inhibitor protein kinase RNA activated (PKR) (Ahmad et al., 2018; Chung et al., 2018; Pestal et al., 2015). Ectopic expression of MDA5 in $ADAR^{KO}$, but not in $ADAR^{WT}$ or parental cells, induced strong activation of an IFN-β reporter (Figure 1B), confirming these results. MDA5 expression in $ADAR^{Z\alpha mut}$ cells similarly resulted in an elevated IFN-β promotor activity albeit less robustly than in $ADAR^{KO}$ cells (Figure 1B). The increased IFN response was specific for MDA5, as overexpression of TRIF, an adaptor molecule for Toll-like receptor (TLR)3/TLR4-mediated IFN-I induction, induced equal responses regardless of the *ADAR* genotype (Figure S1C). This suggests that endogenous agonists of MDA5 accumulate in $ADAR^{Z\alpha mut}$ cells. Indeed, co-expression of the viral dsRNA-binding proteins NS1 from influenza A or E3L from vaccinia virus, but not the dsRNA-binding mutant proteins, prevented the MDA5-induced IFN response (Figure 1C).

Next, we tested whether a spontaneous PKR response occurred in $ADAR^{Z\alpha mut}$ cells. As reported previously (Chung et al., 2018), IFN-α2 treatment of $ADAR^{KO}$ cells induced strong activation of the kinase activity of PKR as shown by PKR autophosphorylation on threonine 451 and serine 51 phosphorylation of the of α subunit of its substrate eukaryotic initiation factor 2 (eIF2α) at 24 and/or 48 h after stimulation (Figures 1D and S1D). Zα domain mutation led to a small increase in activation of PKR compared to cells expressing wild-type ADAR1, only at 48 h after IFN-α2 treatment (Figures 1D and S1D). Phosphorylation of eIF2α by PKR halts initiation of protein translation and promotes selective induction of ATF4-dependent genes (Donnelly et al., 2013). In line with the increase in PKR activation, we detected mildly enhanced mRNA expression of the ATF4 target genes *DDIT3*, *GADD34*, *S100P*, and *ASNS* in most of the $ADAR^{Z\alpha mut}$ clones after IFN-α2 stimulation (Figure 1E).

Taken together, these data indicate that the interaction between the Zα domain of ADAR1 and Z-RNA suppresses the development of spontaneous MDA5 signaling and to a lesser extent prevents PKR activation.

Adar Zα domain mutant mice develop a spontaneous IFN-I response

Next, we generated *Adar* knockin mice expressing an ADAR1 protein in which we mutated the Zα domain residues N175 and

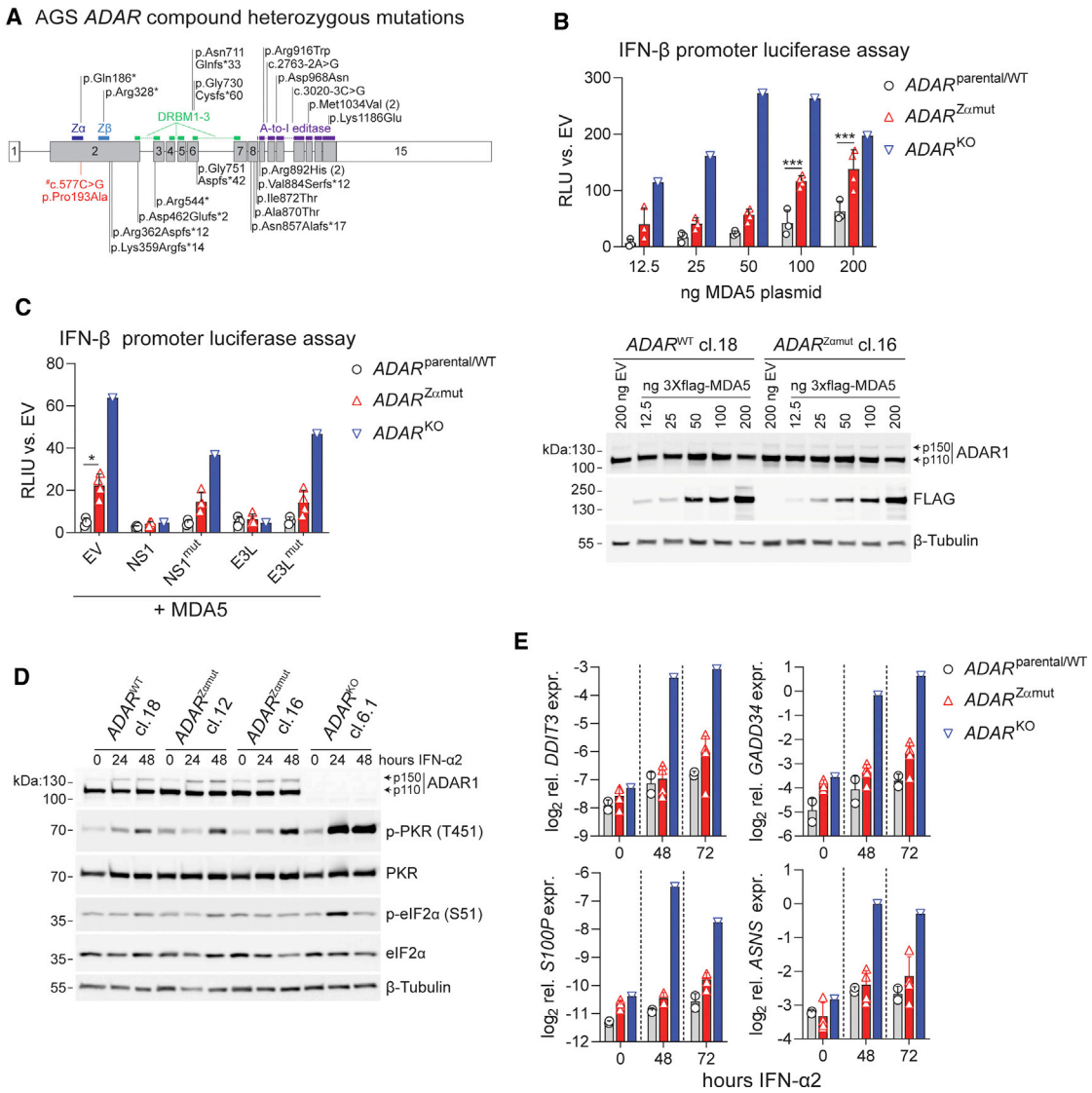

Figure 1. ADAR1 Zα domain mutation activates MDA5 in human cells

(A) Schematic overview of the human *ADAR* gene encoding for ADAR1. Exons are indicated as boxes and introns as lines. The coding sequence is in gray and the 5′ UTR and 3′ UTR are in white. Protein domains including the Z-RNA-binding Zα domain, the Zβ domain, three dsRNA-binding motifs (DRBMs), and the A-to-I editase domain are indicated as colored bars. Compound heterozygous ADAR mutations that occur in patients with AGS are shown. The Zα domain mutation c.577C>G (p.Pro193Ala) is indicated in red. *ADAR* nonsense mutations or missense mutations that are predicted to abrogate the ADAR1 A-to-I editing activity of the other allele are in black.

(B) Parental HEK293 cells or *ADAR* wild-type clones ($ADAR^{parental/WT}$), Zα domain mutant ($ADAR^{Z\alpha mut}$), or ADAR1-deficient ($ADAR^{Z\alpha mut}$) HEK293 clones were transfected with 50 ng of IFN-β promoter-inducible firefly and 20 ng of constitutively active *Renilla* luciferase reporter plasmids, together with increasing amounts of FLAG-tagged human MDA5. Luciferase activity was measured after 24 h, and the relative luciferase units (RLU) were calculated by determining the ratio of firefly and *Renilla* luciferase units. RLU was set to 1 for cells transfected with 200 ng of empty vector. Protein expression of ADAR1 and FLAG-tagged MDA5 in an $ADAR^{WT}$ and $ADAR^{Z\alpha mut}$ clone was verified by western blot (bottom panel). Arrows indicate the ADAR1 p110 and p150 isoforms. ***$p < 0.001$, by two-way ANOVA.

(C) Cells of the indicated genotype were transfected with IFN-β promoter firefly and *Renilla* luciferase reporter plasmids as in (B) and 100 ng of FLAG-tagged human MDA5 together with 100 ng of wild-type NS1 or $NS1^{R38A/K41A}$ ($NS1^{mut}$) from influenza A or wild-type E3L or $E3L^{N44A/Y48A/K167A}$ ($E3L^{mut}$). Luciferase activity was analyzed as in (B). *$p < 0.05$, by unpaired t test. Bars in (B) and (C) represent mean normalized luciferase expression, and symbols represent individual clones.

(D) HEK293 clones of the indicated genotypes were left untreated or stimulated for 24 or 48 h with 1,000 U/mL IFN-α2. Protein expression of ADAR1, threonine 451 (T451) phosphorylated PKR (p-PKR), total PKR, serine 51 (S51) phosphorylated eIF2α (p-eIF2α), and total eIF2α was analyzed by western blotting. Arrows indicate the ADAR1 p110 and p150 isoforms.

(E) qRT-PCR analysis of the indicated ATF4-target genes in the indicated HEK293 cell lines.

Data in (B)–(E) are representative of at least two independent experiments. See also Figure S1.

Y179 into alanines, orthologous to the human N173A/Y177A variations. Because complete ADAR1 and ADAR1-p150 knockout mice die embryonically (Hartner et al., 2004; Wang et al., 2004; Ward et al., 2011), we created conditional ADAR1 Zα domain knockin mice by cloning an inverted mutant Zα domain containing exon 2 downstream of the wild-type sequence. Both the wild-type and mutant exons were flanked by LoxP and Lox2272 sites, enabling Cre-mediated excision of the wild-type exon, and inversion of the mutant exon creates a Zα domain mutant *Adar* allele (*Adar*$^{Z\alpha}$) (Figure S2A). First, we crossed heterozygous conditional Zα domain mutant mice (*Adar*$^{fl\text{-}Z\alpha/+}$) to Sox2-Cre mice, resulting in full body recombination of the floxed allele into a Zα domain mutant allele (Hayashi et al., 2003). The resulting heterozygous *Adar*$^{Z\alpha/+}$ offspring were interbred to generate homozygous *Adar*$^{Z\alpha/Z\alpha}$ mice. Sanger sequencing confirmed successful Cre-mediated recombination (Figure S2B). In contrast to *Adar*$^{-/-}$ and *Adar-p150*$^{-/-}$ mice, *Adar*$^{Z\alpha/Z\alpha}$ animals were born at Mendelian ratios, had no gross defects, and bred normally (Figure S2C). Zα domain mutation did not affect ADAR1 p110 and/or p150 protein expression in bone-marrow-derived macrophages (BMDMs), brain extracts, or lung fibroblasts in resting or IFN-I-stimulated cells (Figures 2A, S2D, and S2E). ADAR1 p110 is a nuclear protein while p150 shuttles between the nucleus and the cytosol. We confirmed that ADAR1 localization did not differ in *Adar*$^{Z\alpha/Z\alpha}$ or control fibroblasts (Figure S2E).

As the Zα domain of ADAR1 is required to suppress MDA5-mediated IFN-I induction in human cells, we analyzed mRNA expression of the IFN-stimulated genes (ISGs) *Ifi44*, *Isg15*, and *Zbp1* in *Adar*$^{Z\alpha/Z\alpha}$ cells. While overnight BMDM or lung fibroblast cultures did not develop an IFN-I response (Figures S2F and S2G), we detected a strong IFN-I gene signature when *Adar*$^{Z\alpha/Z\alpha}$ lung fibroblasts were cultured for 1 week (Figure 2B). This delayed response most likely depended on a feedforward loop induced by the autocrine secretion of IFN-Is. Indeed, *Adar*$^{Z\alpha/Z\alpha}$ cells produced increased levels of CXCL10 protein, a sensitive surrogate marker for IFN-I (Figure 2C). Analysis of *Ifi44* and *Isg15* expression across several tissues of 8- to 10-week-old mice, including heart, lung, spleen, liver, and kidney, also revealed an IFN-I gene signature in *Adar*$^{Z\alpha/Z\alpha}$ animals (Figure 2D). In line with this, we detected enhanced levels of CXCL10 in serum and elevated protein expression of the ISG ZBP1 in brain, spleen, and lung tissue (Figures 2E, S2D, and S2H) of *Adar*$^{Z\alpha/Z\alpha}$ animals.

Similar to human cells, ADAR1 deficiency in mouse cells also leads to spontaneous PKR activation and triggers an unfolded protein response (UPR) during mesenchymal-to-epithelial transition (George et al., 2016; Guallar et al., 2020). To determine whether ADAR1 Zα domain mutation triggers PKR/ATF4 activation and/or induces a UPR, we measured mRNA expression of the ATF4-target genes *Asns* and *Ddit3* and UPR-induced transcripts, including *BiP* (or *Hspa5*) and *Xbp1*, in the unspliced (*Xbp1u*) and spliced (*Xbp1s*) forms in the lungs of *Adar*$^{Z\alpha/Z\alpha}$ mice (Figure S2I). In contrast to the robust IFN-I signature (Figure 2D), we did not find evidence for PKR or UPR activation.

We then asked whether various cell types reacted differentially to loss of ADAR1/Z-RNA interactions. We therefore sorted CD45^{+} leukocytes including alveolar macrophages, neutrophils, conventional type 1 and type 2 dendritic cells (cDC1 and cDC2), and CD45^{-} endothelial and epithelial cells from lungs (Figures S3A and S3B), as well as B cells, T cells, and natural killer (NK) cells from spleens (Figure S3C) of *Adar*$^{Z\alpha/Z\alpha}$ mice. Analysis of mRNA expression of multiple ISGs showed that the Zα domain of ADAR1 is essential to suppress a spontaneous IFN-I response in all tested cell types, although the magnitude of the response differed between cell types (Figures S3D and S3E). Neutrophils, lung epithelium, and lung endothelial cells displayed a particularly robust IFN-I signature (Figure S3D). It remains to be determined whether all of these cell types act as source of IFN-Is or that they respond to elevated circulating IFN-Is. RNA sequencing (RNA-seq) of fluorescence-activated cell sorting (FACS)-purified lung endothelial cells confirmed that loss of ADAR1 interaction with Z-RNA triggered a spontaneous IFN-I response. The top 25 upregulated differentially expressed genes were ISGs (Figure 2F; Table S1), and Gene Ontology (GO) enrichment analysis did not reveal any signs of activation of other immune pathways (Figure 2G).

We conclude that disruption of the interaction between ADAR1 and Z-RNA triggers a systemic IFN-I response and does not lead to a detectable activation of PKR or a UPR.

Adar$^{Z\alpha/Z\alpha}$ mice develop a MAVS-dependent IFN-I response

To test whether the spontaneous IFN-I response caused by ADAR1 Zα domain mutation depended on the MDA5/MAVS signaling pathway, we crossed *Adar*$^{Z\alpha/Z\alpha}$ mice to animals that are deficient for MAVS, an essential signaling adaptor for the RIG-I like receptors (RLRs) RIG-I and MDA5 (Kawai et al., 2005; Meylan et al., 2005; Seth et al., 2005; Xu et al., 2005). As expected, *Adar*$^{Z\alpha/Z\alpha}$ mice displayed increased *Ifi44* and *Isg15* mRNA expression in lung, spleen, and brain; however, ADAR1 Zα domain mutant animals that were deficient for MAVS did not develop an IFN-I signature (Figures 3A–3C). Based on our observation that mutation of the ADAR1 Zα domain triggers an MDA5-mediated IFN-I response in human cells (see Figure 1) and the fact that the embryonic lethality of *Adar*$^{-/-}$ mice is rescued in an MDA5-deficient background, but not by RIG-I deficiency (Pestal et al., 2015), we conclude that the spontaneous antiviral immune response is driven by MDA5/MAVS. Finally, to determine whether the enhanced IFN-I response of *Adar*$^{Z\alpha/Z\alpha}$ mice provides protection against viruses, we infected Zα domain mutant mice and control littermates with encephalomyocarditis virus (EMCV), a positive-stranded RNA virus that is recognized by MDA5 (Gitlin et al., 2006). We detected reduced copies of EMCV RNA in the hearts of *Adar*$^{Z\alpha/Z\alpha}$ mice compared to control animals (Figure 3D). ADAR1 has been reported to act as a proviral factor for influenza, measles, and HIV-1 (Clerzius et al., 2009; Doria et al., 2009; Vogel et al., 2020; Ward et al., 2011). The antiviral effect of ADAR1 Zα domain mutation was abrogated in *Adar*$^{Z\alpha/Z\alpha}$ mice in a MAVS-deficient background, showing that the MAVS-mediated chronic antiviral state rather than an impaired proviral function of ADAR1 protected *Adar*$^{Z\alpha/Z\alpha}$ mice against EMCV.

Adar$^{Z\alpha/Z\alpha}$ mice maintain normal hematopoiesis and do not develop autoinflammatory disease

Loss of ADAR1 activity results in severe defects in hematopoietic development, which is largely driven by spontaneous activation

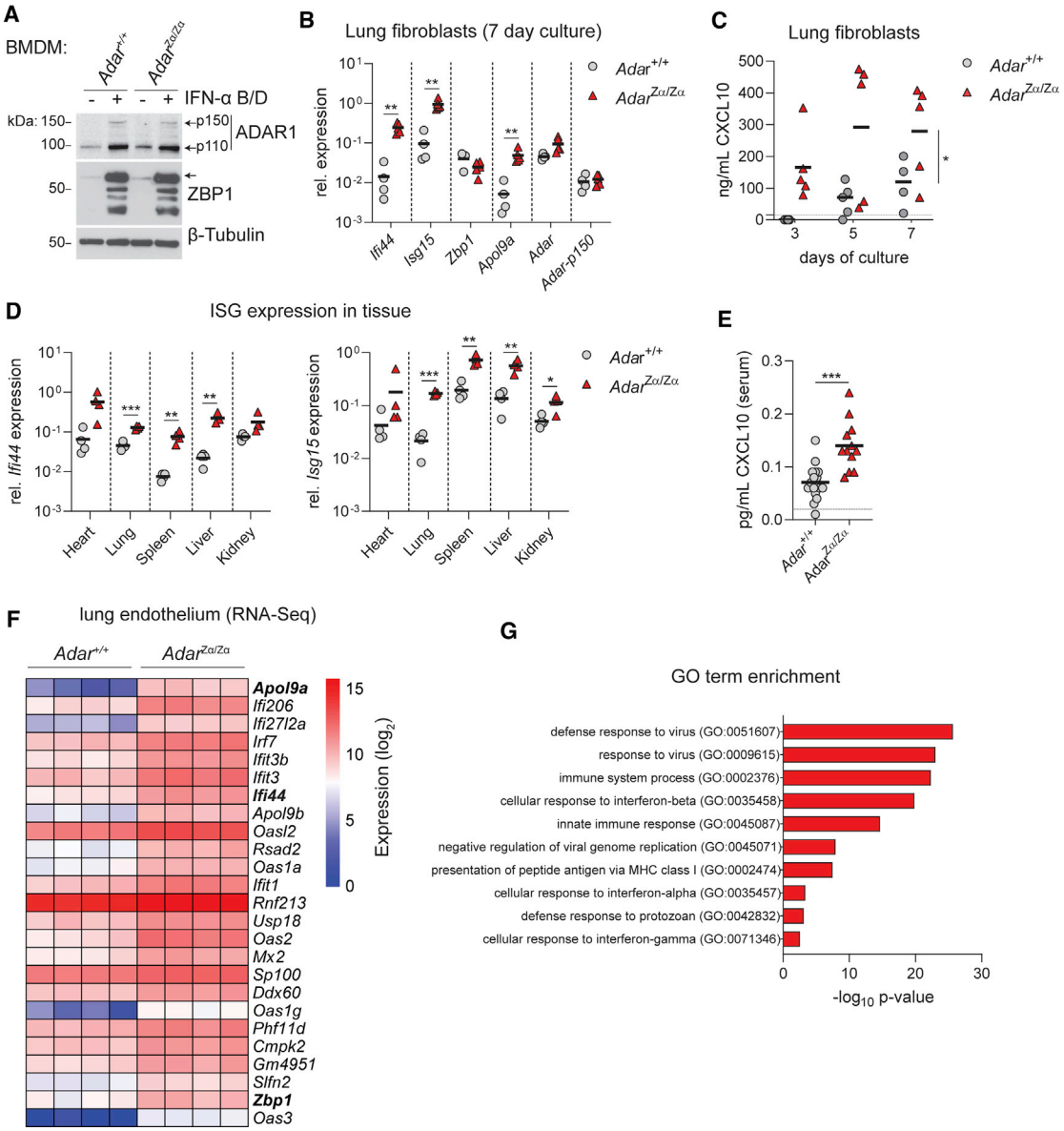

Figure 2. *Adar* Zα domain mutant mice develop a spontaneous IFN-I response

(A) Bone-marrow-derived macrophages (BMDMs) from wild-type (*Adar*$^{+/+}$) and ADAR1 Zα domain mutant (*Adar*$^{Zα/Zα}$) mice were left untreated or stimulated for 18 h with 200 U/mL IFN-α B/D. Protein expression of ADAR1 (isoforms p110 and p150) and ZBP1 was analyzed by western blot.

(B and C) Primary lung fibroblasts from *Adar*$^{+/+}$ and *Adar*$^{Zα/Zα}$ mice were cultured without medium change for 7 days. (B) qRT-PCR analysis of the indicated ISGs at day 7 of the culture. **p < 0.01, by unpaired t test. (C) CXCL10 protein levels in the cell culture supernatant were measured on days 3, 5, and 7 by ELISA. *p < 0.05, by two-way ANOVA. Each data point in (B) and (C) represents a fibroblast culture from an individual mouse. Lines indicate the mean.

(D) qRT-PCR analysis of *Ifi44* and *Isg15* in the indicated organs of 8- to 10-week-old *Adar*$^{+/+}$ and *Adar*$^{Zα/Zα}$ mice. *p < 0.05, **p < 0.01, ***p < 0.001, by unpaired t test.

(E) Analysis of CXCL10 protein levels in serum of 16-week-old *Adar*$^{+/+}$ and *Adar*$^{Zα/Zα}$ mice by Bio-Plex assay. ***p < 0.001, by Mann-Whitney U test. Each data point in (D) and (E) represents an individual mouse. Lines indicate the mean.

(F) Log_2-normalized expression levels of top 25 (total, n = 152; see Table S1) differentially expressed genes (DEGs) identified by total stranded RNA-seq data from primary lung endothelial cells of *Adar*$^{+/+}$ (n = 4) and *Adar*$^{Zα/Zα}$ (n = 4) mice.

(G) Gene Ontology (GO) enrichment analysis of all 152 DEGs identified in (F) by the functional annotation tool of DAVID with Bonferroni correction. *p < 0.05, by Mann-Whitney U test.

Data in (A)–(E) are representative of at least two independent experiments. See also Figures S2 and S3.

of MDA5 (Hartner et al., 2009; Liddicoat et al., 2015, 2016). To determine whether hematopoiesis was affected in *Adar*$^{Zα/Zα}$ mice, we performed whole-blood phenotyping and detailed flow cytometry analyses of the leukocyte compartment of 8- to 10-week-old mice. *Adar*$^{Zα/Zα}$ mice were mildly anemic as indicated by the reduced red blood cell numbers and hematocrit

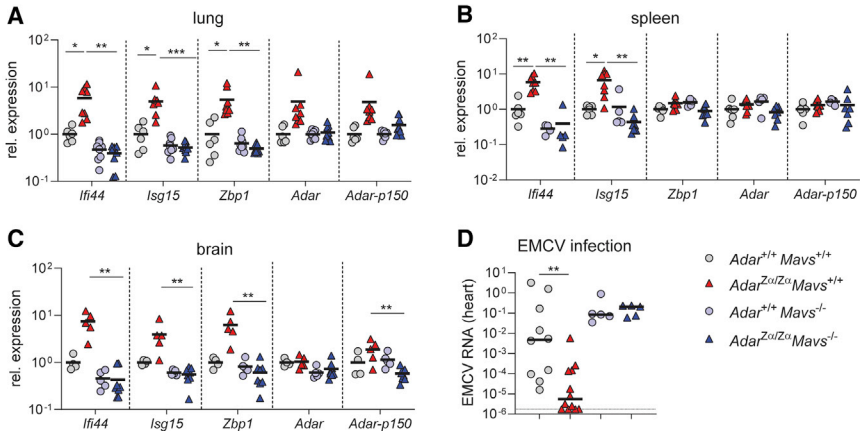

Figure 3. *Adar*$^{Zα/Zα}$ mice develop a MAVS-dependent IFN-I response

(A–C) qRT-PCR analysis of the indicated ISGs in lung (A), spleen (B), and brain (C) tissue from 8-to 10-week-old wild-type and ADAR1 Zα domain mutant mice in a MAVS-sufficient (*Adar*$^{+/+}$ *Mavs*$^{+/+}$ or *Adar*$^{Zα/Zα}$ *Mavs*$^{+/+}$) and MAVS-deficient (*Adar*$^{+/+}$ *Mavs*$^{-/-}$ or *Adar*$^{Zα/Zα}$ *Mavs*$^{-/-}$) background. Data are pooled from two independent experiments. The mean relative expression of each gene in *Adar*$^{+/+}$ *Mavs*$^{+/+}$ tissues is set at 1.

(D) Mice of the indicated genotypes were infected with 2,000 plaque forming units (PFU) of EMCV. At 3 days post-infection, viral titers were determined in the hearts by qRT-PCR of EMCV RNA.

Lines represent the mean, and symbols represent individual mice. *p < 0.05. **p < 0.01, ***p < 0.001, by unpaired t test.

and hemoglobin levels (Figure S4A). We did not detect any differences in the numbers of circulating lymphocytes (B cells, CD4 and CD8 T cells, and NK and NK T cells) or myeloid cells (neutrophils, basophils, eosinophils, and Ly-6C$^-$ and Ly-6C$^+$ monocytes) (Figures S4B and S4C). Taken together, this suggests that disrupted ADAR1/Z-RNA interaction has no effect on leukocyte cell development. Interestingly, Ly-6C$^+$ monocytes expressed higher levels of CD64 also known as Fcγ receptor 1 (Figure 4A). The Interferome database categorizes CD64 as an ISG, and monocyte expression of CD64 strongly correlates with circulating IFN-I levels in systemic lupus erythematosus (SLE) patients (Li et al., 2010). Moreover, anemia is a common symptom of SLE (Aringer, 2020). Both the increased expression of CD64 and reduced presence of red blood cells therefore suggest that *Adar*$^{Zα/Zα}$ mice may be prone to the development of SLE-like autoimmune disease. We did not detect any notable increase in the number of GL7$^+$CD95$^+$ germinal center B cells, plasmablasts, and CD3ε$^+$CD4/CD8$^-$B220$^+$ nonconventional T cells or a reduction in Foxp3$^+$ regulatory CD4 T cells (Tregs) in the spleens of *Adar*$^{Zα/Zα}$ mice (Figures S4D and S4E), which are indicative for autoimmunity development (Kool et al., 2011). Despite the absence of these autoimmune markers, the spleens of ADAR1 Zα domain mutant mice contained fewer naive CD64L^{hi}CD44$^-$ and more activated CD64L^{hi}CD44$^+$ central memory CD8 T cells, while CD4 T cells were unaffected (Figure 4B).

To determine whether *Adar*$^{Zα/Zα}$ mice develop autoimmunity later in life, we housed a cohort of *Adar*$^{Zα/Zα}$ animals and littermate controls until 1 year of age. Despite the fact that *Adar*$^{Zα/Zα}$ males were leaner than their wild-type littermates (Figure 4C), we did not observe any macroscopic signs of disease. Instead, we found that the increase in ISG expression was less pronounced in the brains of 1-year-old *Adar*$^{Zα/Zα}$ mice compared to younger animals (Figure 4D; compare to Figure 3C). In accordance with the loss of the IFN-I signature in older animals, we detected similar levels of CXCL10 protein in serum of 1-year-old *Adar*$^{Zα/Zα}$ and control littermates (Figure S4F). Aged ADAR1 Zα domain mutant mice still showed enhanced CD8 T cell activation (Figure 4E); however, we did not observe an abnormal expansion of GC B cells, plasmablasts, or CD3ε$^+$CD4/CD8$^-$B220$^+$ T cells or a reduction in Tregs in the spleens of these animals (Figure S4G).

Taken together, these results show that *Adar*$^{Zα/Zα}$ mice develop normally without a breach in T or B cell tolerance. The systemically elevated IFN-I signature that is evident in 8- to 10-week-old animals is not sustained until 1 year of age, suggesting that a chronic exposure to IFN-Is is tolerated until later in life without the development of autoinflammatory disease.

Loss of ADAR1/Z-RNA interaction results in reduced A-to-I editing of SINEs

To understand the molecular mechanism that drives the spontaneous IFN-I response when the Z-RNA binding capacity of ADAR1 is abrogated, we asked whether the A-to-I editing activity of ADAR1 is disrupted in Zα domain mutant cells. A-to-I sites can be determined bioinformatically from RNA-seq data, as inosines are interpreted as guanosines by reverse transcriptase during cDNA synthesis, thereby introducing A-to-G (A>G) RNA-DNA differences (RDDs). We first determined A>G RDDs in the RNA-seq dataset from mouse lung endothelial cells (see Figures 2F and 2G). We identified 20,534 unique A-to-I editing sites in mouse lung endothelium from the combined transcriptomes of four *Adar*$^{Zα/Zα}$ and four control samples. Most of these sites were located in introns followed by 3′ UTRs (Figure 5A). RepeatMasker analysis revealed that more than half of these sites mapped to repeat elements and that 60% of the repeat targets were located in SINEs, mostly B1 and B2 repeats (Figure 5A), which is in agreement with previously determined mouse A-to-I editing profiles (Licht et al., 2019; Neeman et al., 2006; Tan et al., 2017). 13,590 sites were found in both Zα domain mutant and wild-type cells. We also identified 2,472 non-overlapping wild-type-only sites and 4,472 sites that were only found in lung endothelium from *Adar*$^{Zα/Zα}$ mice (Figure 5B). It is important to note that the likelihood of uncovering A-to-I sites is largely a function of sequencing depth (Bazak et al., 2014). This is especially problematic when dealing with sites that are edited at low levels and that would require a proportionally higher read coverage for their reliable detection. We can therefore not exclude that part of the sites identified as Zα domain mutant-only or wild-type-only were falsely assigned to these groups due to a lack in sequencing coverage. To avoid dealing with this bias we decided to only consider sites that were common to at least two wild-type and two Zα domain mutant samples, generating

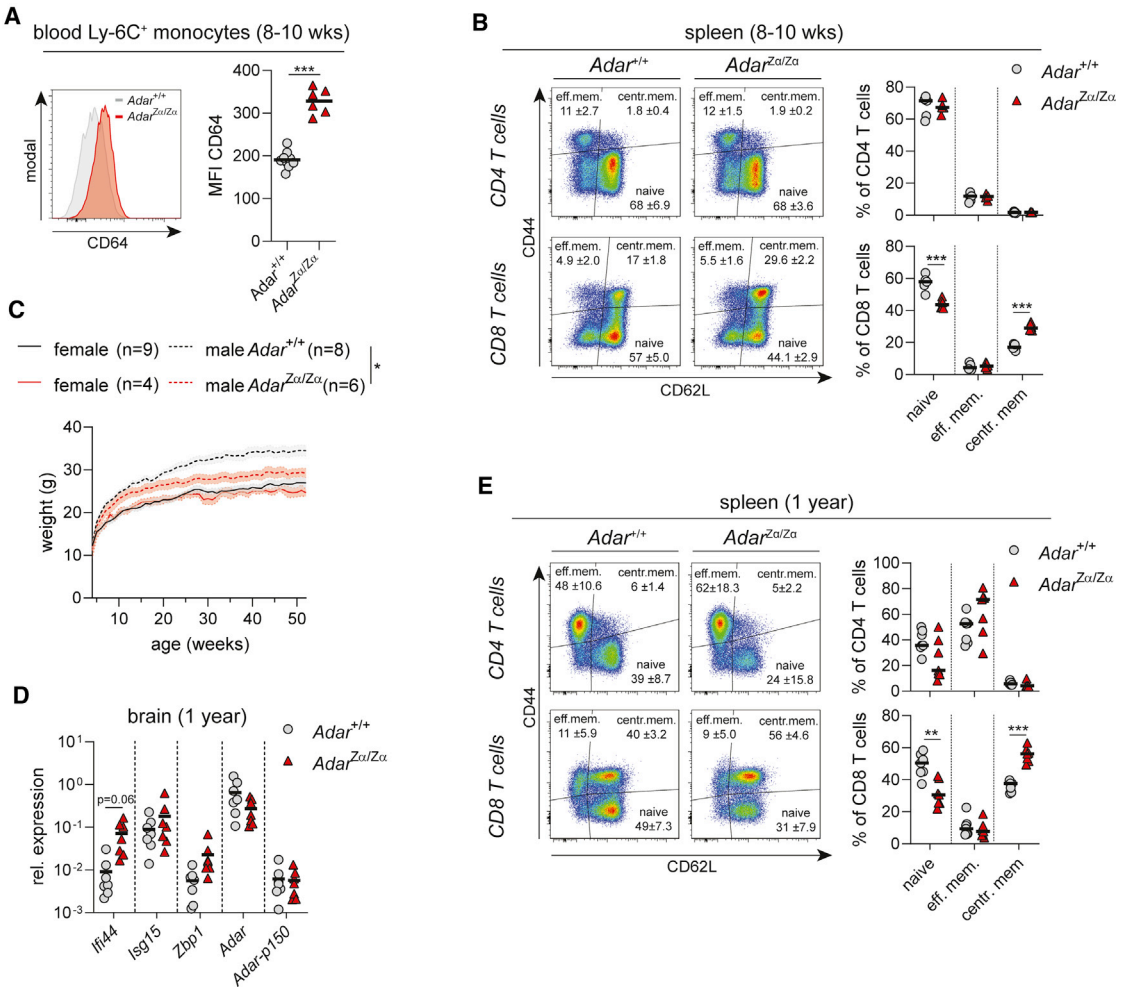

Figure 4. *Adar*$^{Zα/Zα}$ mice maintain normal hematopoiesis and do not develop autoinflammatory disease

(A) Peripheral blood from 8- to 10-week-old *Adar*$^{Zα/Zα}$ mice and their wild-type littermates (*Adar*$^{+/+}$) was analyzed by flow cytometry. The histogram (left) depicts representative CD64 expression levels on Ly-6C^{+} monocytes. Quantification of CD64 expression levels on Ly-6C^{+} monocytes by median fluorescence intensity (MFI; right). The gating strategy is outlined in Figure S4B. Lines represent the mean, and dots indicate individual mice. ***p < 0.001, by Mann-Whitney U test.

(B) Splenic CD4 and CD8 T cells from 8- to 10-week-old mice from the indicated genotypes were analyzed for CD44 and CD62L expression by flow cytometry. Gating of naive (CD44^{-}CD62L^{lo}) and activated effector memory (eff.mem.; CD44^{hi}CD62L^{lo}) and central memory (centr.mem.; CD44^{+}CD62L^{hi}) CD4 and CD8 T cells are indicated by representative flow cytometry plots (left) for each genotype. Quantification is shown of naive and activated CD4 and CD8 T cell subpopulations as percentage of the total population (right). The gating strategy is outlined in Figure S4D. Lines represents the mean, and symbols depict individual mice. ***p < 0.001, by unpaired t test.

(C) Weight in grams (g) of male and female mice of the indicated genotype was measured weekly from 4 until 52 weeks of age. Lines represent mean, and shaded area shows ± SEM. *p < 0.05, by two-way ANOVA.

(D) qRT-PCR analysis of the indicated ISGs in brain tissue from the 1-year-old *Adar*$^{+/+}$ and *Adar*$^{Zα/Zα}$ mice. Lines represents the mean, and symbols depict individual mice. p = 0.06 by unpaired t test.

(E) Spleens from 1-year-old mice of the indicate genotype were analyzed as in (B). Lines represents the mean, and symbols depict individual mice. **p < 0.01, ***p < 0.001, by unpaired t test.

See also Figure S4.

2,907 high-confidence A-to-I editing sites (Figure 5B). We then measured the efficiency of ADAR1 editing by calculating the A-to-I editing index for each of these targets, which represents the number of reads containing an edited adenosine relative to the total number of reads covering that particular site. We found that the overall editing efficiency was reduced in cells expressing the Zα domain mutant variant of ADAR1 (Figure 5C). This was evident for sites covering the whole transcript including targets within 3′ UTRs, introns, and 5′ UTRs and exons, annotated as "other" (Figure 5D). Deeper analysis showed that a larger fraction of sites was less efficiently edited in most SINE family members. This suggests that Zα domain mutation led to an overall reduction in ADAR1 editing efficiency rather than affecting specific SINEs (Figure S5B). Importantly, we did not observe any major differences in transcript abundance of different repeat sequence families including the SINE/B1 and SINE/B2 elements

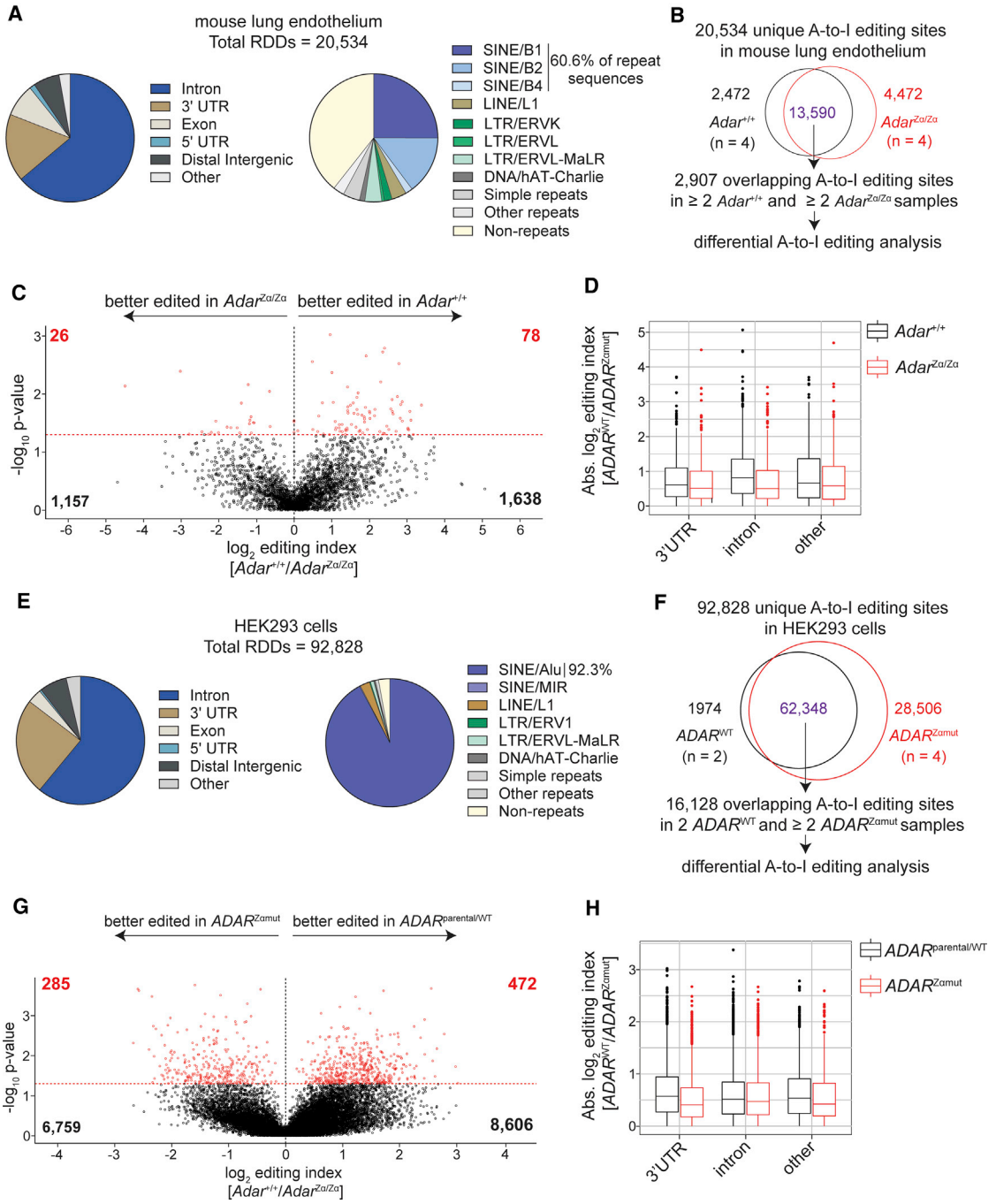

Figure 5. Loss of ADAR1/Z-RNA interaction results in reduced A-to-I editing of SINEs

(A) A total of 20,534 unique A-to-I editing sites (≥10 read coverage) were determined using total stranded RNA-seq data obtained from FACS-purified lung endothelial cells of *Adar*$^{+/+}$ (n = 4) and *Adar*$^{Z\alpha/Z\alpha}$ (n = 4) mice. Genomic (left) and RepeatMasker (right) annotations of the A-to-I sites are presented as pie charts.

(B) Flowchart of the analysis pipeline to determine sites that are differentially edited between wild-type and ADAR1 Zα domain mutant transcriptomes. Differential editing analysis was performed on sites that were identified in at least two *Adar*$^{+/+}$ and at least two *Adar*$^{Z\alpha/Z\alpha}$ samples.

(C and D) Volcano plot (C) and boxplot (D) showing differential A-to-I editing in primary lung endothelial cells of *Adar*$^{+/+}$ and *Adar*$^{Z\alpha/Z\alpha}$ mice. The editing index of each site is the number of variant reads containing an A>G RDD by the total number of reads covering the site. Significance of differential editing (y axis in C) was determined by applying a Welch two-sample t test on the $\log_{10}$ editing index values of each sample for every site. The $\log_2$ editing index (x axis in C) of each site was calculated by dividing the mean editing index in *Adar*$^{+/+}$ samples by the mean editing index in *Adar*$^{Z\alpha/Z\alpha}$ samples followed by $\log_2$ transformation. Positive values indicate a higher editing index in the wild-type samples. The y axis in (D) displays the absolute editing index of sites that were better edited in wild-type samples (black boxes) versus Zα domain mutant samples (red boxes) subdivided according to their genomic annotation.

(legend continued on next page)

between genotypes, showing that the difference in editing efficiency was not due to differential repeat expression (Figure S5A).

We then performed the same analysis in *ADAR*$^{Z\alpha mut}$ HEK293 cells (see Figure S1B). ADAR1-p150 is lowly expressed in HEK293 cells and its expression is induced by IFN-I treatment (see Figure 1D). To study the effect of Zα domain mutation of ADAR1 on its A-to-I editing activity, we induced the expression of ADAR1-p150 by stimulating cells with IFN-α2. We refined our analysis by removing false-positive editing sites occurring in *ADAR*^{KO} cells and removed A>G RDDs that were annotated as single nucleotide polymorphisms in the parental HEK293 cells (Lin et al., 2014) (Figure S5C). In line with previous findings (Chung et al., 2018; Pfaller et al., 2018), we found that overall A-to-I editing was reduced in *ADAR-p150*^{KO} cells; however, we identified an equal number of sites in *ADAR*$^{Z\alpha mut}$ and control cells (Figure S5C). We determined 92,828 unique A-to-I sites from the combined transcriptomes of two control and four *ADAR*$^{Z\alpha mut}$ samples. Similar to mouse endothelium, most of these sites mapped to introns and 3′ UTRs, and more than 90% of editing sites were located in SINE/*Alu* repeats (Figure 5E), which is in agreement with other studies in human cells (Athanasiadis et al., 2004; Blow et al., 2004; Kim et al., 2004; Levanon et al., 2004). We identified 16,128 overlapping targets that were present in the two control samples and at least two *ADAR*$^{Z\alpha mut}$ samples (Figure 5F). We found that (similar to mouse cells) a larger fraction of sites was better edited in wild-type cells than in *ADAR*$^{Z\alpha mut}$ cells (Figure 5G). This was not a consequence of differential repeat expression, as ADAR1 Zα domain mutation did not alter repeat RNA levels (Figure S5D). In contrast to mouse endothelium, we found that intronic sites were relatively unaffected by loss of Z-RNA interaction with ADAR1 while the reduction in editing efficiency was most pronounced in 3′ UTRs (Figure 5H). Again, the reduction in editing efficiency of Zα domain mutant ADAR1 could not be attributed to a loss of activity toward a single or multiple SINE/*Alu* family members (Figure S5E).

Altogether, these results show that Z-RNA binding to ADAR1 promotes A-to-I editing of SINEs. In human transcripts, introns remained relatively unaffected by loss of ADAR1 activity, while in mouse endothelium this affected the whole transcript. This suggests that the enhanced IFN-I signature due to Zα domain mutation of ADAR1 is driven by the recognition of SINE-derived duplex RNA by MDA5.

Compound heterozygous *Adar*$^{Z\alpha/null}$ mice die postnatally and develop a severe MAVS-dependent IFN-I response

AGS resulting from compound heterozygous *ADAR* mutations is caused by pairing of a P193A Zα domain mutant variant with a dysfunctional *ADAR* allele (Rice et al., 2017). We noted that the embryonic development of homozygous *Adar*$^{fl\text{-}Z\alpha/fl\text{-}Z\alpha}$ mice was impaired at embryonic day 11.5 (E11.5) (Figure S6A). *Adar*$^{fl\text{-}Z\alpha/fl\text{-}Z\alpha}$ embryos also displayed increased ISG expression, and ADAR1-p150 was not expressed in embryonic extracts (Figures S6B and S6C). *Adar*$^{fl\text{-}Z\alpha/fl\text{-}Z\alpha}$ mice recapitulate the phenotype of complete ADAR1 or ADAR1-p150 deficient animals, which die embryonically at E11.5–E12.5 and develop a MDA5/MAVS-dependent IFN-I response (Mannion et al., 2014; Pestal et al., 2015). The *Adar*$^{fl\text{-}Z\alpha}$ allele thus constitutes an *Adar*(*-p150*) null variant, hereafter referred to as *Adar*^{null}. This is most likely the result of disrupted splicing due to insertion of an inverted Zα domain mutant exon downstream of the wild-type sequence (see Figure S2A). To mimic the compound heterozygous state of patients with AGS, we crossed *Adar*$^{Z\alpha/Z\alpha}$ mice to *Adar*$^{null/+}$ mice, thereby generating *Adar*$^{Z\alpha/null}$ mice that express Zα domain mutant ADAR1 only from one allele. Although *Adar*$^{Z\alpha/null}$ offspring were alive at birth, as evidenced by the presence of milk in their stomachs, they were smaller and less than half of the pups survived beyond postnatal day 0.5 (P0.5) and the remaining animals died by P1.5 (Figures 6A, 6B, and S6D). We measured high levels of CXCL10 in the serum of P0.5 *Adar*$^{Z\alpha/null}$ mice, but at this stage in development, we did not detect increased CXCL10 levels in pups expressing Zα domain mutant ADAR1 from both alleles (Figure 6C). ISG mRNA expression was enhanced in the brains, lungs, and intestines of *Adar*$^{Z\alpha/null}$ pups (Figures 6D and S6F). Genetic removal of MAVS from *Adar*$^{Z\alpha/null}$ mice restored viability at least until 14 weeks of life and prevented the development of a spontaneous IFN-I response (Figures 6B, 6D, S6E, and S6F).

Taken together, these data show that while expression of a Zα domain mutant ADAR1 protein from both alleles is viable, hemizygous expression leads to a lethal MAVS-dependent phenotype.

DISCUSSION

Around 1 million copies of the ~300-bp SINE/*Alu* repeat element occupy the human genome, thereby constituting around 11% of the total DNA content (Deininger, 2011; Lander et al., 2001). Human *Alu* elements and mouse B1 and B2 repeats are enriched in genes and are especially prevalent in introns and 3′ UTRs (Lu et al., 2020). Given their sheer abundance, SINEs are thought to have a profound impact on cell function and direct processes such as transcription, histone modification, and gene evolution (Burns and Boeke, 2012; Lee et al., 2015). It is estimated that one new *Alu* insertion occurs every 20 births (Cordaux et al., 2006). The acquisition of SINEs inside genes may generate genomic plasticity; however, it comes at the risk of invoking an unwanted immune response (Kassiotis and Stoye, 2016; Mu et al., 2016). Transcripts that contain two adjacent and oppositely oriented SINEs can form dsRNA structures. Computational

(E) A total of 92,828 unique A-to-I editing sites (≥10 read coverage) were determined using total stranded RNA-seq data obtained from *ADAR*$^{WT/parental}$ (n = 2) and *ADAR*$^{Z\alpha/Z\alpha}$ (n = 4) HEK293 cells. Genomic (left) and RepeatMasker (right) annotations of the A-to-I sites are presented as pie charts.
(F) Flowchart of the analysis pipeline to determine sites that are differentially edited between wild-type and ADAR1 Zα domain mutant transcriptomes. Differential editing analysis was performed on sites that were identified in *ADAR*$^{WT/parental}$ and at least two *ADAR*$^{Z\alpha/Z\alpha}$ samples.
(G and H) Volcano plot (G) and boxplot (H) showing differential A-to-I editing in wild-type and ADAR1 Zα domain mutant HEK293 cells calculated using the same approach as in (C) and (D).
See also Figure S5.

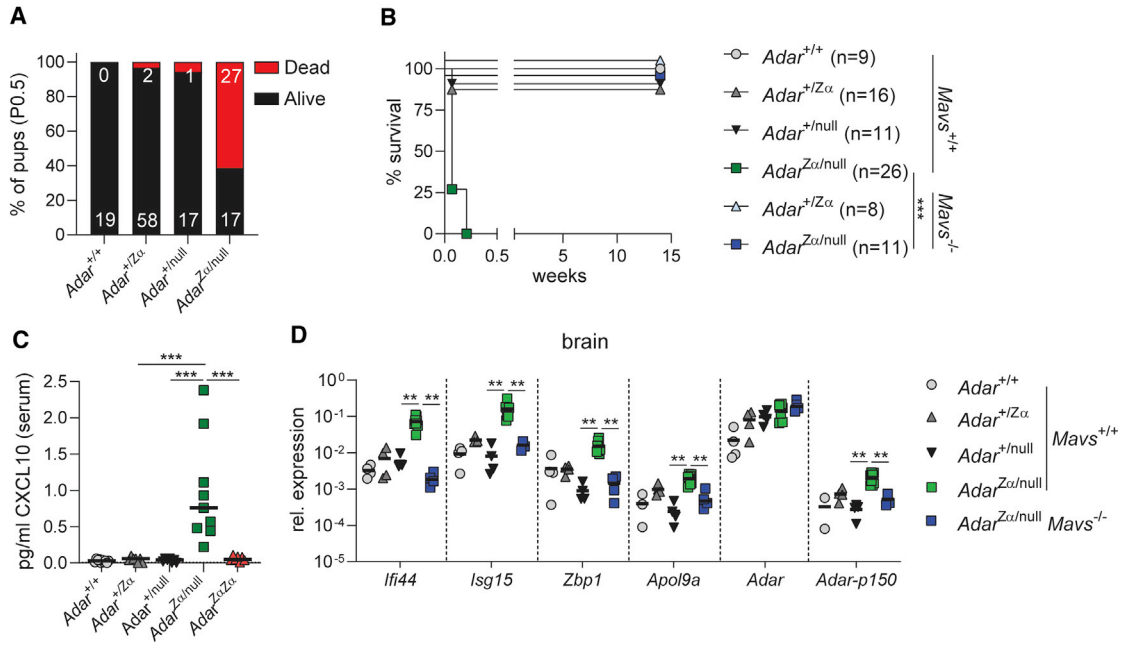

Figure 6. Compound heterozygous *Adar*$^{Z\alpha/null}$ mice die postnatally and develop a severe MAVS-dependent IFN-I response

Adar$^{+/null}$ mice were crossed to *Adar*$^{+/+}$ or *Adar*$^{Z\alpha/Z\alpha}$ animals to generate *Adar*$^{+/+}$, *Adar*$^{+/null}$, *Adar*$^{+/Z\alpha}$, or *Adar*$^{Z\alpha/null}$ offspring, and *Adar*$^{+/null}$ *Mavs*$^{-/-}$ mice were crossed to *Adar*$^{Z\alpha/Z\alpha}$ *Mavs*$^{-/-}$ animals to generate *Adar*$^{+/Z\alpha}$ *Mavs*$^{-/-}$ or *Adar*$^{+/null}$ *Mavs*$^{-/-}$ offspring.

(A) Survival of pups of the indicated genotypes at P0.5. The numbers in the bar chart depict the number of live or dead pups.

(B) Kaplan-Meier survival curve of offspring of the indicated genotypes. ***$p < 0.001$, by log-rank test.

(C) Analysis of CXCL10 protein levels in serum of P0.5 pups of the indicated genotypes.

(D) qRT-PCR analysis of the indicated ISGs in brain tissue from P0.5 mice of the indicated genotypes. Lines in (C) and (D) represent the mean, and symbols depict individual mice. **$p < 0.01$, ***$p < 0.001$, by unpaired t test.

See also Figure S6.

analysis on the orientation of repeat elements and their likelihood to form dsRNA across species revealed that there is a strong selection against the presence of neighboring inversely oriented repeat sequences in the 3′ UTR of mRNAs, but not in intron-containing precursor mRNAs (Barak et al., 2020). Purifying selection against dsRNA structures is incomplete, and inverted SINE repeats that have escaped this process may activate MDA5. Ultra-deep sequencing revealed that nearly every adenosine in *Alu* elements with a potential to form dsRNA is subject to the A-to-I editing activity of ADAR1 (Bazak et al., 2014). ADAR1 activity thus forms a second barrier to prevent deleterious MDA5 activation by SINE-derived dsRNA molecules.

The importance of ADAR1 in suppressing MDA5-mediated immunity is evident from patients with AGS carrying loss-of-function mutations in *ADAR* (Rice et al., 2012). In this study, we focused on the observation that more than half of these patients carried the p.Pro193Ala mutation in combination with a dysfunctional *ADAR* variant (Rice et al., 2017). Proline 193 lies within the Z-RNA binding Zα domain of the p150-isoform of ADAR1, and its mutation is predicted to disrupt ADAR1/Z-RNA interaction. These patients thus hemizygously express a mutant ADAR1 protein that is unable to interact with Z-RNA. This implies that the interaction between the poorly defined Z conformer of dsRNA and ADAR1 is required to fully exert its immunosuppressive effects. Indeed, Zα domain mutation led to reduced ADAR1 activity measured by an editing reporter plasmid, and *in vitro* ADAR1-p150 activity was enhanced toward a synthetic Z-RNA-containing dsRNA substrate (Koeris et al., 2005; Mannion et al., 2014; Wong et al., 2003). In this study, we performed a transcriptome-wide analysis of thousands of A-to-I sites in human and mouse cells that express Zα domain mutant ADAR1 and found that the overall editing efficiency was reduced by loss of ADAR1/Z-RNA interaction. While the reduction in ADAR1 activity in mouse cells applied to whole transcripts, this was particularly evident for 3′ UTRs in human transcripts, which is in agreement with a recent study (Sun et al., 2021). As introns are spliced out before nuclear export, SINE-derived dsRNA structures in 3′ UTRs are most likely responsible for the activation of the cytosolic dsRNA sensor MDA5. The Zα domain containing ADAR1-p150 isoform shuttles between the nucleus and the cytosol, and hence an important part of its immunosuppressive effect may be to modify dsRNA structures in 3′ UTRs of mRNAs that were recently exported out of the nucleus. We noted that some transcripts were better edited in cells expressing Zα domain mutant ADAR1. This may result from the redirection of ADAR1 from Z-RNA-containing dsRNA molecules toward ‘‘classical’’ A-form dsRNA helices. Nonetheless, the increased activity toward these substrates was not sufficient to suppress an IFN-I response, suggesting that endogenous Z-RNA-containing transcripts have immunostimulatory potential and may drive autoinflammatory disease.

The identity of the RNA sequences that form Z-RNA remains unknown. The capacity of dsRNA to transition into the thermodynamically unfavorable Z conformation is dependent on the sequence context. A 6-bp r(GC)$_3$ RNA duplex forms the minimum Zα domain recognition motif, at least *in vitro* (Placido et al., 2007). The Zα domain of ADAR1 could in theory bind to any dsRNA structure containing such a motif. Indeed, putative Z-RNA-forming sequences were annotated in *Alu* repeats (Herbert, 2019). Moreover, recent studies in mice reported that SINE-derived duplex RNA may serve as an endogenous ligand for the Z-RNA sensor ZBP1, the only mammalian protein aside from ADAR1 that contains a Zα domain (Jiao et al., 2020; Wang et al., 2020). We were not able to discern one or more members of the human *Alu* and mouse B1/B2 elements that were particularly "hypo-edited" due to Zα domain mutation. A specific combination of inverted SINE pairs may be more prone to form Z-RNA. In order to determine these Z-RNA-forming motifs, we would need to determine each SINE in relation to its inversely oriented partner. To identify these combinations, one could employ the recently developed MDA5 RNase protection/RNA-seq method (Ahmad et al., 2018) or perform ADAR1 cross-linking and immunoprecipitation sequencing (CLIP-seq).

Homozygous *Adar*$^{Z\alpha/Z\alpha}$ mice display a subclinical IFN-I response and do not develop AGS-like pathology even at 1 year of age. Patients with AGS express the Pro193Ala ADAR1 variant only from one allele, suggesting that gene dosage is an important factor in dictating disease development. Indeed, *Adar*$^{Z\alpha/null}$ mice that express half the amount of ADAR1 Zα domain mutant protein developed a pathological IFN-I response and died after birth, confirming this unique genotypic-phenotypic relationship. The missense *ADAR* p.Pro193ala mutation has an unusually high allele frequency of ~0.2%, suggesting that this variant may offer an evolutionary advantage. We found that *Adar*$^{Z\alpha/Z\alpha}$ mice were more resistant to virus infection. It is possible that heterozygous carriers of the p.Pro193ala allele produce elevated levels of IFN-Is to better deal with viral insults. Genetic mutations resulting in subclinically elevated IFN-I levels may thus prime the immune system for future infections.

In sum, we provide evidence that Z-RNA binding to ADAR1 is crucial to maintain tolerance to self-RNA. We propose that ADAR1/Z-RNA interactions widen the editing repertoire of ADAR1 and that disruption of this interaction leads to the accumulation of immunostimulatory SINE-derived dsRNA that may trigger the onset of human autoinflammatory diseases such as AGS.

STAR★METHODS

Detailed methods are provided in the online version of this paper and include the following:

SUPPLEMENTAL INFORMATION

Supplemental information can be found online at https://doi.org/10.1016/j.celrep.2021.109500.

ACKNOWLEDGMENTS

We would like to thank Wim Declercq for helpful discussions and critical reading of the manuscript. We are grateful to A. Wullaert for providing *Mavs*$^{-/-}$ mice, to E. Picardi for providing the mouse A-to-I editing site positive training dataset for RDDpred (Licht et al., 2019), the VIB Protein Core for recombinant Cas9-GFP, and to the VIB-UGent IRC Animal House for mouse husbandry. We would like to thank the VIB Flow Core for training, support, and access to the instrument park. This research would not have been possible without support from the following funding agencies. R.d.R. was supported by a Ghent University BOF PhD fellowship (01D24020). L.S. was supported by an FWO postdoctoral fellowship (1236420N). Research in the Vandenabeele group is supported by EOS MODEL-IDI (FWO grant 30826052), FWO research grants (G.0E04.16N, G.0C76.18N, G.0B71.18N, and G.0B96.20N), Methusalem (BOF16/MET_V/007), the Foundation Against Cancer (F/2016/865 and F/2020/1505), CRIG and GIGG consortia, and VIB. J.M. was supported by an Odysseus II Grant (G0H8618N) from the Research Foundation Flanders and by Ghent University.

AUTHOR CONTRIBUTIONS

Conceptualization, R.d.R., E.D., and J.M.; methodology, R.d.R., E.D., B.W., K.S., F.V.N., and J.M.; software, R.d.R., T.M., and A.B.; formal analysis, R.d.R.; investigation, R.d.R., E.D., B.W., K.S., L.S., E.D.M., and J.M.; resources, B.N.L., F.V.N., P.V., and J.M.; writing – original draft, R.d.R. and J.M.; writing – review & editing, R.d.R. and J.M.; funding acquisition, R.d.R. and J.M.; supervision, J.M.

DECLARATION OF INTERESTS

The authors declare no competing interests.

Received: December 4, 2020
Revised: May 14, 2021
Accepted: July 15, 2021
Published: August 10, 2021

REFERENCES

Ahmad, S., Mu, X., Yang, F., Greenwald, E., Park, J.W., Jacob, E., Zhang, C.Z., and Hur, S. (2018). Breaching self-tolerance to Alu duplex RNA underlies MDA5-mediated inflammation. Cell *172*, 797–810.e13.

Anders, S., Pyl, P.T., and Huber, W. (2015). HTSeq–a Python framework to work with high-throughput sequencing data. Bioinformatics *31*, 166–169.

Aringer, M. (2020). Inflammatory markers in systemic lupus erythematosus. J. Autoimmun. *110*, 102374.

Athanasiadis, A., Rich, A., and Maas, S. (2004). Widespread A-to-I RNA editing of Alu-containing mRNAs in the human transcriptome. PLoS Biol. *2*, e391.

Bajad, P., Ebner, F., Amman, F., Szabó, B., Kapoor, U., Manjali, G., Hildebrandt, A., Janisiw, M.P., and Jantsch, M.F. (2020). An internal deletion of ADAR rescued by MAVS deficiency leads to a minute phenotype. Nucleic Acids Res. *48*, 3286–3303.

Barak, M., Porath, H.T., Finkelstein, G., Knisbacher, B.A., Buchumenski, I., Roth, S.H., Levanon, E.Y., and Eisenberg, E. (2020). Purifying selection of long dsRNA is the first line of defense against false activation of innate immunity. Genome Biol. *21*, 26.

Bazak, L., Haviv, A., Barak, M., Jacob-Hirsch, J., Deng, P., Zhang, R., Isaacs, F.J., Rechavi, G., Li, J.B., Eisenberg, E., and Levanon, E.Y. (2014). A-to-I RNA editing occurs at over a hundred million genomic sites, located in a majority of human genes. Genome Res. *24*, 365–376.

Blow, M., Futreal, P.A., Wooster, R., and Stratton, M.R. (2004). A survey of RNA editing in human brain. Genome Res. *14*, 2379–2387.

Bolger, A.M., Lohse, M., and Usadel, B. (2014). Trimmomatic: a flexible trimmer for Illumina sequence data. Bioinformatics *30*, 2114–2120.

Burns, K.H., and Boeke, J.D. (2012). Human transposon tectonics. Cell *149*, 740–752.

Bylund, L., Kytölä, S., Lui, W.O., Larsson, C., and Weber, G. (2004). Analysis of the cytogenetic stability of the human embryonal kidney cell line 293 by cytogenetic and STR profiling approaches. Cytogenet. Genome Res. *106*, 28–32.

Chung, H., Calis, J.J.A., Wu, X., Sun, T., Yu, Y., Sarbanes, S.L., Dao Thi, V.L., Shilvock, A.R., Hoffmann, H.H., Rosenberg, B.R., and Rice, C.M. (2018). Human ADAR1 prevents endogenous RNA from triggering translational shutdown. Cell *172*, 811–824.e14.

Clerzius, G., Gélinas, J.F., Daher, A., Bonnet, M., Meurs, E.F., and Gatignol, A. (2009). ADAR1 interacts with PKR during human immunodeficiency virus infection of lymphocytes and contributes to viral replication. J. Virol. *83*, 10119–10128.

Cordaux, R., Hedges, D.J., Herke, S.W., and Batzer, M.A. (2006). Estimating the retrotransposition rate of human Alu elements. Gene *373*, 134–137.

Crow, Y.J., Chase, D.S., Lowenstein Schmidt, J., Szynkiewicz, M., Forte, G.M., Gornall, H.L., Oojageer, A., Anderson, B., Pizzino, A., Helman, G., et al. (2015). Characterization of human disease phenotypes associated with mutations in *TREX1*, *RNASEH2A*, *RNASEH2B*, *RNASEH2C*, *SAMHD1*, *ADAR*, and *IFIH1*. Am. J. Med. Genet. A. *167A*, 296–312.

Deininger, P. (2011). Alu elements: Know the SINEs. Genome Biol. *12*, 236.

Devos, M., Tanghe, G., Gilbert, B., Dierick, E., Verheirstraeten, M., Nemegeer, J., de Reuver, R., Lefebvre, S., De Munck, J., Rehwinkel, J., et al. (2020). Sensing of endogenous nucleic acids by ZBP1 induces keratinocyte necroptosis and skin inflammation. J. Exp. Med. *217*, e20191913.

Dobin, A., Davis, C.A., Schlesinger, F., Drenkow, J., Zaleski, C., Sonali, J., Batut, P., Chaisson, M., and Gingeras, T.R. (2013). STAR: ultrafast universal RNA-seq aligner. Bioinformatics *29*, 15–21.

Donnelly, N., Gorman, A.M., Gupta, S., and Samali, A. (2013). The eIF2α kinases: Their structures and functions. Cell. Mol. Life Sci. *70*, 3493–3511.

Doria, M., Neri, F., Gallo, A., Farace, M.G., and Michienzi, A. (2009). Editing of HIV-1 RNA by the double-stranded RNA deaminase ADAR1 stimulates viral infection. Nucleic Acids Res. *37*, 5848–5858.

Feng, S., Li, H., Zhao, J., Pervushin, K., Lowenhaupt, K., Schwartz, T.U., and Dröge, P. (2011). Alternate rRNA secondary structures as regulators of translation. Nat. Struct. Mol. Biol. *18*, 169–176.

Fletcher, A.L., Malhotra, D., Acton, S.E., Lukacs-Kornek, V., Bellemare-Pelletier, A., Curry, M., Armant, M., and Turley, S.J. (2011). Reproducible isolation of lymph node stromal cells reveals site-dependent differences in fibroblastic reticular cells. Front. Immunol. *2*, 35.

Gao, B., Huang, Q., and Baudis, M. (2018). segment_liftover : a Python tool to convert segments between genome assemblies. F1000Research *7:319*.

George, C.X., Ramaswami, G., Li, J.B., and Samuel, C.E. (2016). Editing of cellular self-RNAs by adenosine deaminase ADAR1 suppresses innate immune stress responses. J. Biol. Chem. *291*, 6158–6168.

Gitlin, L., Barchet, W., Gilfillan, S., Cella, M., Beutler, B., Flavell, R.A., Diamond, M.S., and Colonna, M. (2006). Essential role of mda-5 in type I IFN responses to polyriboinosinic:polyribocytidylic acid and encephalomyocarditis picornavirus. Proc. Natl. Acad. Sci. USA *103*, 8459–8464.

Guallar, D., Fuentes-Iglesias, A., Souto, Y., Ameneiro, C., Freire-Agulleiro, O., Pardavila, J.A., Escudero, A., Garcia-Outeiral, V., Moreira, T., Saenz, C., et al. (2020). ADAR1-dependent RNA editing promotes MET and iPSC reprogramming by alleviating ER stress. Cell Stem Cell *27*, 300–314.e11.

Hartner, J.C., Schmittwolf, C., Kispert, A., Müller, A.M., Higuchi, M., and Seeburg, P.H. (2004). Liver disintegration in the mouse embryo caused by deficiency in the RNA-editing enzyme ADAR1. J. Biol. Chem. *279*, 4894–4902.

Hartner, J.C., Walkley, C.R., Lu, J., and Orkin, S.H. (2009). ADAR1 is essential for the maintenance of hematopoiesis and suppression of interferon signaling. Nat. Immunol. *10*, 109–115.

Hayashi, S., Tenzen, T., and McMahon, A.P. (2003). Maternal inheritance of Cre activity in a *Sox2Cre* deleter strain. Genesis *37*, 51–53.

Herbert, A. (2019). Z-DNA and Z-RNA in human disease. Commun. Biol. *2*, 7.

Jiao, H., Wachsmuth, L., Kumari, S., Schwarzer, R., Lin, J., Eren, R.O., Fisher, A., Lane, R., Young, G.R., Kassiotis, G., et al. (2020). Z-nucleic-acid sensing triggers ZBP1-dependent necroptosis and inflammation. Nature *580*, 391–395.

Kassiotis, G., and Stoye, J.P. (2016). Immune responses to endogenous retroelements: Taking the bad with the good. Nat. Rev. Immunol. *16*, 207–219.

Kawai, T., Takahashi, K., Sato, S., Coban, C., Kumar, H., Kato, H., Ishii, K.J., Takeuchi, O., and Akira, S. (2005). IPS-1, an adaptor triggering RIG-I- and Mda5-mediated type I interferon induction. Nat. Immunol. *6*, 981–988.

Kesavardhana, S., Kuriakose, T., Guy, C.S., Samir, P., Malireddi, R.K.S., Mishra, A., and Kanneganti, T.D. (2017). ZBP1/DAI ubiquitination and sensing of influenza vRNPs activate programmed cell death. J. Exp. Med. *214*, 2217–2229.

Kesavardhana, S., Malireddi, R.K.S., Burton, A.R., Porter, S.N., Vogel, P., Pruett-Miller, S.M., and Kanneganti, T.D. (2020). The Zα2 domain of ZBP1 is a molecular switch regulating influenza-induced PANoptosis and perinatal lethality during development. J. Biol. Chem. *295*, 8325–8330.

Kim, D.D., Kim, T.T., Walsh, T., Kobayashi, Y., Matise, T.C., Buyske, S., and Gabriel, A. (2004). Widespread RNA editing of embedded alu elements in the human transcriptome. Genome Res. *14*, 1719–1725.

Kim, M.S., Hur, B., and Kim, S. (2016). RDDpred: A condition-specific RNA-editing prediction model from RNA-seq data. BMC Genomics *17* (*Suppl 1*), 5.

Kiran, A.M., O'Mahony, J.J., Sanjeev, K., and Baranov, P.V. (2013). Darned in 2013: Inclusion of model organisms and linking with Wikipedia. Nucleic Acids Res. *41*, D258–D261.

Koeris, M., Funke, L., Shrestha, J., Rich, A., and Maas, S. (2005). Modulation of ADAR1 editing activity by Z-RNA in vitro. Nucleic Acids Res. *33*, 5362–5370.

Kool, M., van Loo, G., Waelput, W., De Prijck, S., Muskens, F., Sze, M., van Praet, J., Branco-Madeira, F., Janssens, S., Reizis, B., et al. (2011). The ubiquitin-editing protein A20 prevents dendritic cell activation, recognition of apoptotic cells, and systemic autoimmunity. Immunity *35*, 82–96.

Kuhn, R.M., Haussler, D., and Kent, W.J. (2013). The UCSC genome browser and associated tools. Brief. Bioinform. *14*, 144–161.

Lander, E.S., Linton, L.M., Birren, B., Nusbaum, C., Zody, M.C., Baldwin, J., Devon, K., Dewar, K., Doyle, M., FitzHugh, W., et al.; International Human Genome Sequencing Consortium (2001). Initial sequencing and analysis of the human genome. Nature *409*, 860–921.

Lee, H.E., Ayarpadikannan, S., and Kim, H.S. (2015). Role of transposable elements in genomic rearrangement, evolution, gene regulation and epigenetics in primates. Genes Genet. Syst. *90*, 245–257.

Levanon, E.Y., Eisenberg, E., Yelin, R., Nemzer, S., Hallegger, M., Shemesh, R., Fligelman, Z.Y., Shoshan, A., Pollock, S.R., Sztybel, D., et al. (2004). Systematic identification of abundant A-to-I editing sites in the human transcriptome. Nat. Biotechnol. *22*, 1001–1005.

Li, H., Handsaker, B., Wysoker, A., Fennell, T., Ruan, J., Homer, N., Marth, G., Abecasis, G., and Durbin, R.; 1000 Genome Project Data Processing Subgroup (2009). The Sequence Alignment/Map format and SAMtools. Bioinformatics *25*, 2078–2079.

Li, Y., Lee, P.Y., Kellner, E.S., Paulus, M., Switanek, J., Xu, Y., Zhuang, H., Sobel, E.S., Segal, M.S., Satoh, M., and Reeves, W.H. (2010). Monocyte surface expression of Fcγ receptor RI (CD64), a biomarker reflecting type-I interferon levels in systemic lupus erythematosus. Arthritis Res. Ther. *12*, R90.

Licht, K., Kapoor, U., Amman, F., Picardi, E., Martin, D., Bajad, P., and Jantsch, M.F. (2019). A high resolution A-to-I editing map in the mouse identifies editing events controlled by pre-mRNA splicing. Genome Res. *29*, 1453–1463.

Liddicoat, B.J., Piskol, R., Chalk, A.M., Ramaswami, G., Higuchi, M., Hartner, J.C., Li, J.B., Seeburg, P.H., and Walkley, C.R. (2015). RNA editing by ADAR1 prevents MDA5 sensing of endogenous dsRNA as nonself. Science *349*, 1115–1120.

Liddicoat, B.J., Hartner, J.C., Piskol, R., Ramaswami, G., Chalk, A.M., Kingsley, P.D., Sankaran, V.G., Wall, M., Purton, L.E., Seeburg, P.H., et al. (2016). Adenosine-to-inosine RNA editing by ADAR1 is essential for normal murine erythropoiesis. Exp. Hematol. *44*, 947–963.

Lin, Y.C., Boone, M., Meuris, L., Lemmens, I., Van Roy, N., Soete, A., Reumers, J., Moisse, M., Plaisance, S., Drmanac, R., et al. (2014). Genome dynamics of the human embryonic kidney 293 lineage in response to cell biology manipulations. Nat. Commun. *5*, 4767.

Love, M.I., Huber, W., and Anders, S. (2014). Moderated estimation of fold change and dispersion for RNA-seq data with DESeq2. Genome Biology *15*, 550.

Lu, J.Y., Shao, W., Chang, L., Yin, Y., Li, T., Zhang, H., Hong, Y., Percharde, M., Guo, L., Wu, Z., et al. (2020). Genomic repeats categorize genes with distinct functions for orchestrated regulation. Cell Rep. *30*, 3296–3311.e5.

Maelfait, J., Liverpool, L., Bridgeman, A., Ragan, K.B., Upton, J.W., and Rehwinkel, J. (2017). Sensing of viral and endogenous RNA by ZBP1/DAI induces necroptosis. EMBO J. *36*, 2529–2543.

Mannion, N.M., Greenwood, S.M., Young, R., Cox, S., Brindle, J., Read, D., Nellåker, C., Vesely, C., Ponting, C.P., McLaughlin, P.J., et al. (2014). The RNA-editing enzyme ADAR1 controls innate immune responses to RNA. Cell Rep. *9*, 1482–1494.

Mansi, L., Tangaro, M.A., Lo Giudice, C., Flati, T., Kopel, E., Schaffer, A.A., Castrignano, T., Chillemi, G., Pesole, G., and Picardi, E. (2021). REDIportal: Millions of novel A-to-I RNA editing events from thousands of RNAseq experiments. Nucleic Acids Res. *49* (*D1*), D1012–D1019.

Meylan, E., Curran, J., Hofmann, K., Moradpour, D., Binder, M., Bartenschlager, R., and Tschopp, J. (2005). Cardif is an adaptor protein in the RIG-I antiviral pathway and is targeted by hepatitis C virus. Nature *437*, 1167–1172.

Michallet, M.C., Meylan, E., Ermolaeva, M.A., Vazquez, J., Rebsamen, M., Curran, J., Poeck, H., Bscheider, M., Hartmann, G., König, M., et al. (2008). TRADD protein is an essential component of the RIG-like helicase antiviral pathway. Immunity *28*, 651–661.

Mu, X., Ahmad, S., and Hur, S. (2016). Endogenous retroelements and the host innate immune sensors. Adv. Immunol. *132*, 47–69.

Neeman, Y., Levanon, E.Y., Jantsch, M.F., and Eisenberg, E. (2006). RNA editing level in the mouse is determined by the genomic repeat repertoire. RNA *12*, 1802–1809.

Pestal, K., Funk, C.C., Snyder, J.M., Price, N.D., Treuting, P.M., and Stetson, D.B. (2015). Isoforms of RNA-editing enzyme ADAR1 independently control nucleic acid sensor MDA5-driven autoimmunity and multi-organ development. Immunity *43*, 933–944.

Pfaller, C.K., Donohue, R.C., Nersisyan, S., Brodsky, L., and Cattaneo, R. (2018). Extensive editing of cellular and viral double-stranded RNA structures accounts for innate immunity suppression and the proviral activity of ADAR1^{p150}. PLoS Biol. *16*, e2006577.

Placido, D., Brown, B.A., 2nd, Lowenhaupt, K., Rich, A., and Athanasiadis, A. (2007). A left-handed RNA double helix bound by the Z alpha domain of the RNA-editing enzyme ADAR1. Structure *15*, 395–404.

Ramaswami, G., and Li, J.B. (2014). RADAR: A rigorously annotated database of A-to-I RNA editing. Nucleic Acids Res. *42*, D109–D113.

Rice, G.I., Kasher, P.R., Forte, G.M., Mannion, N.M., Greenwood, S.M., Szynkiewicz, M., Dickerson, J.E., Bhaskar, S.S., Zampini, M., Briggs, T.A., et al. (2012). Mutations in *ADAR1* cause Aicardi-Goutières syndrome associated with a type I interferon signature. Nat. Genet. *44*, 1243–1248.

Rice, G.I., Kitabayashi, N., Barth, M., Briggs, T.A., Burton, A.C.E., Carpanelli, M.L., Cerisola, A.M., Colson, C., Dale, R.C., Danti, F.R., et al. (2017). Genetic, phenotypic, and interferon biomarker status in ADAR1-related neurological disease. Neuropediatrics *48*, 166–184.

Rodero, M.P., and Crow, Y.J. (2016). Type I interferon-mediated monogenic autoinflammation: The type I interferonopathies, a conceptual overview. J. Exp. Med. *213*, 2527–2538.

Schade, M., Turner, C.J., Lowenhaupt, K., Rich, A., and Herbert, A. (1999). Structure-function analysis of the Z-DNA-binding domain Zalpha of dsRNA adenosine deaminase type I reveals similarity to the (alpha + beta) family of helix-turn-helix proteins. EMBO J. *18*, 470–479.

Schwartz, T., Rould, M.A., Lowenhaupt, K., Herbert, A., and Rich, A. (1999). Crystal structure of the Zalpha domain of the human editing enzyme ADAR1 bound to left-handed Z-DNA. Science *284*, 1841–1845.

Seth, R.B., Sun, L., Ea, C.K., and Chen, Z.J. (2005). Identification and characterization of MAVS, a mitochondrial antiviral signaling protein that activates NF-kappaB and IRF 3. Cell *122*, 669–682.

Sridharan, H., Ragan, K.B., Guo, H., Gilley, R.P., Landsteiner, V.J., Kaiser, W.J., and Upton, J.W. (2017). Murine cytomegalovirus IE3-dependent transcription is required for DAI/ZBP1-mediated necroptosis. EMBO Rep. *18*, 1429–1441.

Sun, T., Yu, Y., Wu, X., Acevedo, A., Luo, J.D., Wang, J., Schneider, W.M., Hurwitz, B., Rosenberg, B.R., Chung, H., and Rice, C.M. (2021). Decoupling expression and editing preferences of ADAR1 p150 and p110 isoforms. Proc. Natl. Acad. Sci. USA *118*, e2021757118.

Tan, M.H., Li, Q., Shanmugam, R., Piskol, R., Kohler, J., Young, A.N., Liu, K.I., Zhang, R., Ramaswami, G., Ariyoshi, K., et al.; GTEx Consortium; Laboratory, Data Analysis &Coordinating Center (LDACC)—Analysis Working Group; Statistical Methods groups—Analysis Working Group; Enhancing GTEx (eGTEx) groups; NIH Common Fund; NIH/NCI; NIH/NHGRI; NIH/NIMH; NIH/NIDA; Biospecimen Collection Source Site—NDRI; Biospecimen Collection Source Site—RPCI; Biospecimen Core Resource—VARI; Brain Bank Repository—University of Miami Brain Endowment Bank; Leidos Biomedical—Project Management; ELSI Study; Genome Browser Data Integration &Visualization—EBI; Genome Browser Data Integration &Visualization—UCSC Genomics Institute, University of California Santa Cruz (2017). Dynamic landscape and regulation of RNA editing in mammals. Nature *550*, 249–254.

Uggenti, C., Lepelley, A., Depp, M., Badrock, A.P., Rodero, M.P., El-Daher, M.T., Rice, G.I., Dhir, S., Wheeler, A.P., Dhir, A., et al. (2020). cGAS-mediated induction of type I interferon due to inborn errors of histone pre-mRNA processing. Nat. Genet. *52*, 1364–1372.

Vogel, O.A., Han, J., Liang, C.Y., Manicassamy, S., Perez, J.T., and Manicassamy, B. (2020). The p150 isoform of ADAR1 blocks sustained RLR signaling and apoptosis during influenza virus infection. PLoS Pathog. *16*, e1008842.

Wang, Q., Miyakoda, M., Yang, W., Khillan, J., Stachura, D.L., Weiss, M.J., and Nishikura, K. (2004). Stress-induced apoptosis associated with null mutation of *ADAR1* RNA editing deaminase gene. J. Biol. Chem. *279*, 4952–4961.

Wang, R., Li, H., Wu, J., Cai, Z.Y., Li, B., Ni, H., Qiu, X., Chen, H., Liu, W., Yang, Z.H., et al. (2020). Gut stem cell necroptosis by genome instability triggers bowel inflammation. Nature *580*, 386–390.

Ward, S.V., George, C.X., Welch, M.J., Liou, L.Y., Hahm, B., Lewicki, H., de la Torre, J.C., Samuel, C.E., and Oldstone, M.B. (2011). RNA editing enzyme

adenosine deaminase is a restriction factor for controlling measles virus replication that also is required for embryogenesis. Proc. Natl. Acad. Sci. USA *108*, 331–336.

Wong, S.K., Sato, S., and Lazinski, D.W. (2003). Elevated activity of the large form of ADAR1 in vivo: Very efficient RNA editing occurs in the cytoplasm. RNA *9*, 586–598.

Xu, L.G., Wang, Y.Y., Han, K.J., Li, L.Y., Zhai, Z., and Shu, H.B. (2005). VISA is an adapter protein required for virus-triggered IFN-beta signaling. Mol. Cell *19*, 727–740.

Zhang, T., Yin, C., Boyd, D.F., Quarato, G., Ingram, J.P., Shubina, M., Ragan, K.B., Ishizuka, T., Crawford, J.C., Tummers, B., et al. (2020). Influenza virus Z-RNAs induce ZBP1-mediated necroptosis. Cell *180*, 1115–1129.e13.

STAR★METHODS

KEY RESOURCES TABLE

REAGENT or RESOURCE	SOURCE	IDENTIFIER
Antibodies		
Rabbit monoclonal anti-ADAR1 (D7E2M)	Cell Signaling Technology	Cat#14175; RRID: AB_2722520
Mouse monoclonal anti-FLAG M2-Peroxidase (HRP)	Sigma-Aldrich	Cat#A8592; RRID: AB_439702
Rabbit polyclonal anti-β-Tubulin-HRP	Abcam	Cat#ab21058; RRID: AB_727045
Rabbit monoclonal anti-phospho-PKR (T451)	Abcam	Cat#ab81303; RRID: AB_1640780
Rabbit monoclonal anti-PKR	Abcam	Cat#ab32506; RRID: AB_777306
Rabbit monoclonal anti-phospho-eIF2α (S51)	Cell Signaling Technology	Cat#3398; RRID: AB_2096481
Rabbit polyclonal anti-eIF2α	Cell Signaling Technology	Cat#9722; RRID: AB_2230924
Mouse monoclonal anti-Adar1 (15.8.6)	Santa Cruz Biotechnology	Cat#sc-73408; RRID: AB_2222767
Rabbit polyclonal anti-ADAR1-p150	Synaptic Systems GmbH	Cat#293003; RRID: AB_2620031
Mouse monoclonal anti-ZBP1 (Zippy-1)	Adipogen	Cat#AG-20B-0010; RRID: AB_2490191
Mouse monoclonal anti-Histone H1 (AE-4)	Santa Cruz Biotechnology	Cat#sc-8030; RRID: AB_675641
Rabbit TrueBlot: Anti-Rabbit IgG HRP	eBioscience	Cat# 18-8816-33; RRID: AB_469529
Mouse TrueBlot ULTRA: Anti-Mouse Ig HRP	eBioscience	Cat# 18-8817-31; RRID: AB_2610850
BV421 Rat Anti-Mouse Siglec-F	BD Biosciences	Cat#565934; RRID: AB_2739398
Brilliant Violet 711 anti-mouse CD64 (FcγRI)	Biolegend	Cat#139311; RRID: AB_2563846
BV785 anti-mouse Ly-6G Antibody	Biolegend	Cat#127645; RRID: AB_2566317
Brilliant Violet 650 anti-mouse CD11c	Biolegend	Cat#117339; RRID: AB_2562414
Anti-Mouse MHC Class II (I-A/I-E) FITC	eBiosciences	Cat#11-5321-82; RRID: AB_465232
PE anti-mouse/rat XCR1	Biolegend	Cat#148203; RRID: AB_2563842
Anti-Mouse CD172a (SIRP alpha) PerCP-eFluor 710	eBiosciences	Cat#46-1721-82; RRID: AB_10804639
BUV395 Hamster Anti-Mouse CD3e	BD Biosciences	Cat#563565; RRID: AB_2738278
BV605 Mouse Anti-Mouse NK-1.1	BD Biosciences	Cat#563220; RRID: AB_2738077
CD19 Monoclonal Antibody (eBio1D3 (1D3)) PE-Cyanine5	Invitrogen	Cat#15-0193-82; RRID: AB_657672
V450 Rat anti-Mouse CD44	BD Biosciences	Cat#560451; RRID: AB_1645273
CD62L (L-Selectin) Monoclonal Antibody (MEL- 14), FITC	Invitrogen	Cat#11-0621-82; RRID: AB_465109
BUV737 Rat Anti-Mouse CD4	BD Biosciences	Cat#564298; RRID: AB_2738734
PerCP/Cyanine5.5 anti-mouse CD8b Antibody	Biolegend	Cat#126609; RRID: AB_961304
PerCP-Cy5.5 Rat Anti-Mouse CD11b	BD Biosciences	Cat#550993; RRID: AB_394002
Brilliant Violet 785 anti-mouse F4/80 Antibody	Biolegend	Cat#123141; RRID: AB_2563667
BUV737 Rat Anti-Mouse CD5	BD Biosciences	Cat#565273; RRID: AB_2739146
Alexa Fluor 700 Rat anti-Mouse CD45R	BD Biosciences	Cat#557957; RRID: AB_396957
PE Rat Anti-Mouse CD138	BD Biosciences	Cat#553714; RRID: AB_395000
V450 Rat Anti-Mouse IgD	BD Biosciences	Cat#560869; RRID: AB_10564089
Alexa Fluor 488 anti-mouse/human GL7 Antigen (T and B cell Activation Marker) Antibody	Biolegend	Cat#144611; RRID: AB_2563284
Brilliant Violet 785 anti-mouse TER-119/ Erythroid Cells Antibody	Biolegend	Cat#116245; RRID: AB_2650921

(*Continued on next page*)

Continued

REAGENT or RESOURCE	SOURCE	IDENTIFIER
APC/Cy7 anti-mouse TCR β chain Antibody	Biolegend	Cat#109220; RRID: AB_893624
PE-CF594 Hamster Anti-Mouse γδ T Cell Receptor	BD Biosciences	Cat#563532; RRID: AB_2661844
BV605 Rat Anti-Mouse CD25	BD Biosciences	Cat#563061; RRID: AB_2737982
FOXP3 Monoclonal Antibody (FJK-16 s), APC, eBioscience	Invitrogen	Cat#17-5773-82; RRID: AB_469457
Purified Rat Anti-Mouse CD16/CD32 (Mouse BD Fc Block)	BD Biosciences	Cat#553142; RRID: AB_394657
eBioscience Fixable Viability Dye eFluor 506	eBioscience	Cat# 65-0866-14
CD45 Monoclonal Antibody (30-F11), FITC	eBioscience	Cat# 11-0451-82; RRID: AB_465050
CD31 (PECAM-1) Monoclonal Antibody (390), PE-Cyanine7	eBioscience	Cat# 25-0311-82; RRID: AB_2716949
CD326 (EpCAM) Monoclonal Antibody (G8.8), APC	eBioscience	Cat# 17-5791-82; RRID: AB_2716944
PE anti-mouse CD200R3 Antibody [Ba13]	Biolegend	Cat# 142206; RRID: AB_10916520
Bacterial and virus strains		
Encephalomyocarditis virus	ATCC	VR-129B
Chemicals, peptides, and recombinant proteins		
Recombinant Human IFN-α2	Biolegend	Cat#592704
Recombinant IFN-α B/D hybrid	Novartis	Cat#CGP35269
p125-Luc	A gift from J. Rehwinkel lab, Oxford University	N/A
pRL-TK	Promega	E2241
pcDNA3His/V5 control plasmid	A gift from J. Rehwinkel lab, Oxford University	N/A
pcDNA3-3XFLAG-hMDA5	A gift from J. Rehwinkel lab, Oxford University	N/A
pCAGGS-E-hTRIF	BCCM/GeneCorner	LMBP#05226
pLenti6-HA blast-E3L	This manuscript	N/A
pLenti6-HA blast-E3L-N44A/Y48A/K167A	This manuscript	N/A
pcAXL-NS1-WT	A gift from X. Saelens lab, Ghent University	N/A
pcAXL-mNS1-R38AK41A	A gift from X. Saelens lab, Ghent University	N/A
Critical commercial assays		
IP-10/CXCL10 Mouse Matched Antibody Pair	eBioscience	Cat#BMS6018MST
Bio-Plex Pro Mouse Chemokine IP-10 / CXCL10	Bio-Rad	Cat#12002244
Bio-Plex Pro Reagent Kit V	Bio-Rad	Cat#12002798
Bio-Plex Pro Mouse Chemokine Standards	Bio-Rad	Cat#12002796
RNeasy Mini Kit (50)	QIAGEN Benelux B.V.	Cat# 74104
RNeasy Micro Kit (50)	QIAGEN Benelux B.V.	Cat# 74004
Agilent RNA 6000 Pico Kit	Agilent Technologies	Cat# 50671513
TruSeq Stranded Total RNA Library Prep	Illumina	Cat# 20020596
IDT for Illumina – TruSeq RNA UD Indexes	Illumina	Cat# 20020591
Illumina Ribo-Zero Gold rRNA Depletion Kit	Illumina	Cat#20037135
SMARTer Stranded Total RNA-Seq Kit v2 - Pico Input Mammalian	Takara	Cat#634411
Zero Blunt TOPO PCR Cloning Kit	Invitrogen	Cat#450245
Collagenase D	Roche	Cat#11088866001

(*Continued on next page*)

Continued

REAGENT or RESOURCE	SOURCE	IDENTIFIER
Trypsin (2.5%), no phenol red	GIBCO	Cat#15090-046
ACK (Ammonium-Chloride-Potassium) Lysing Buffer 1X	Lonza	Cat#10-548E
Lipofectamine 2000	Invitrogen	Cat#11668-027
Dual-Luciferase Reporter Assay System	Promega	Cat# E1910
Cell Fractionation Kit	Cell Signaling Technology	Cat#9038S
SensiFAST cDNA Synthesis Kit	Bioline	Cat# BIO-65054
SensiFAST SYBR No-ROX Kit	Bioline	Cat# BIO-98005
PrimeTime Gene Expression Master Mix	IDT	Cat#1055771
Dispase II, powder	Invitrogen	Cat#17105-041
Collagenase P	Sigma-Aldrich	Cat#000000011213857001
DNase I	Roche	Cat#1010459001
anti-FITC microbeads	Miltenyi Biotec	Cat#130-048-701
midiMacs type LS separation	Miltenyi Biotec	Cat#130-042-401
1.4 mm Zirconium oxide beads	VWR International	Cat# P000927-LYSK0-A
Deposited data		
RNA-seq data HEK293 cells	This manuscript	https://www.ebi.ac.uk/: PRJEB46065
RNA-seq data mouse lung endothelial cells	This manuscript	https://www.ebi.ac.uk/: PRJEB46161
Experimental models: Cell lines		
HEK293A cells	Lin et al., 2014	N/A
Bone-marrow derived macrophages	This study	N/A
Primary lung fibroblasts	This study	N/A
Experimental models: Organisms/strains		
Adarfl-Zα mice (C57BL/6)	A gift from J. Rehwinkel lab, Oxford University	N/A
Mavs−/− mice (C57BL/6)	A gift from J. Tschopp lab, Lausanne University	N/A
Oligonucleotides		
Listed in Table S2	IDT	N/A
Software and algorithms		
FastQC v0.11.7	Babraham Bioinformatics	https://www.bioinformatics.babraham.ac.uk/projects/fastqc/
Trimmomatic v1.4	Bolger et al., 2014	http://www.usadellab.org/cms/?page=trimmomatic
STAR 2.7.3a	Dobin et al., 2013	https://github.com/alexdobin/STAR
HTSeq 0.11.1	Anders et al., 2015	https://htseq.readthedocs.io/en/release_0.11.1/install.html
DESeq2 1.26.0	Love et al., 2014	https://bioconductor.org/packages/release/bioc/html/DESeq2.html
R (version 3.6.3 - Holding the Windsock)	CRAN-R-project	https://cran.r-project.org/bin/windows/base/old/3.6.3/
RDDpred_v1.1	Kim et al., 2016	http://epigenomics.snu.ac.kr/RDDpred/prior.php
Samtools v1.9	Li et al., 2009	http://samtools.sourceforge.net/
LiftOver	Gao et al., 2018	https://github.com/baudisgroup/segment-liftover
FlowJo v10.7	FlowJo, LLC	https://www.flowjo.com/solutions/flowjo; RRID: SCR_008520

(*Continued on next page*)

Continued

REAGENT or RESOURCE	SOURCE	IDENTIFIER
Other		
Lightcycler 480 system	Roche	N/A
FACSVerse	BD Biosciences	N/A

RESOURCE AVAILABILITY

Lead contact

Further information and requests for resources and reagents should be directed to and will be fulfilled by the lead contact, Jonathan Maelfait (jonathan.maelfait@irc.vib-ugent.be).

Materials availability

All reagents generated in this study are available from the lead contact with a completed materials transfer agreement.

Data and code availability

All data and code supporting the findings of this study are available within the paper or are available from the lead contact upon request. Fastq files from the RNA-seq datasets are available on the European Nucleotide Archive (https://www.ebi.ac.uk/ena/browser/home), accession codes PRJEB46161 and PRJEB46065. This paper does not report original code. Any additional information required to reanalyse the data reported in this paper is available from the lead contact upon request.

EXPERIMENTAL MODEL AND SUBJECT DETAILS

Mice

Adar$^{fl\text{-}Z\alpha}$ mice were generated in C57BL/6 ES cells by Cyagen and were kindly provided by Jan Rehwinkel. An *Adar*$^{+/fl\text{-}Z\alpha}$ male was crossed to a female Sox2-Cre deleter mouse to generate *Adar*$^{+/Z\alpha}$ offspring. Adar$^{+/Z\alpha}$ mice were interbred to generate homozygous ADAR1 Zα domain mutant (*Adar*$^{Z\alpha/Z\alpha}$) animals. *Adar*$^{+/+}$ littermates were used as controls. Sox2-Cre mice were generated in CBA ES cells (Hayashi et al., 2003) and were purchased from The Jackson Laboratory (B6.Cg-*Edil3*$^{Tg(Sox2\text{-}cre)1Amc}$/J). Sox2-Cre animals were backcrossed at least 10 times to a C57BL/6 background. *Mavs*$^{-/-}$ mice were generated in C57BL/6 ES cells and were obtained from the Jurg Tschopp laboratory (Michallet et al., 2008). Mice were housed in individually ventilated cages at the VIB-Ugent Center for Inflammation Research in a specific pathogen-free facility, according to national and institutional guidelines for animal care. Both males and female littermates were included in all experiments. The age of the mice is indicated in the figure legends. All experiments were conducted following approval by the local Ethics Committee of Ghent University.

EMCV infections

8-10 week old *Adar*$^{Z\alpha/Z\alpha}$, *Adar*$^{Z\alpha/Z\alpha}$ *Mavs*$^{-/-}$ and control *Adar*$^{+/+}$ *Mavs*$^{+/+}$ or *Adar*$^{+/+}$ *Mavs*$^{-/-}$ littermates were infected by intraperitoneal injection with 2000 plaque forming units (pfu) of Encephalomyocarditis virus (ATCC VR-129B). 72 hour post-infection, hearts were homogenized with a Precellys 24 Tissue Homogenizer and 1.4 mm Zirconium oxide beads (VWR International; P000927-LYSK0-A) in 1 mL of Trizol reagent (GIBCO BRL; 15596-018), followed by total RNA extraction as described above.

Cell culture

HEK293A, hereafter referred to as HEK293, cells (Lin et al., 2014) were cultured at 37°C and 5% CO_2 in DMEM/F-12 (Dulbecco's Modified Eagle Medium/Nutrient Mixture F-12, GIBCO;31330-038) supplemented with 10% FCS (Bodinco), 2mM glutamine (Lonza; BE17-605F) and 1mM sodium pyruvate (Sigma-Aldrich; S8636). For bone marrow-derived macrophages (BMDMs), femurs and tibia were collected of 8-10-week-old *Adar*$^{Z\alpha/Z\alpha}$ mice and wild-type littermates. Bones were sterilized in 70% ethanol before flushing them with RPMI 1640 medium using a 26G needle. Next, cells were homogenized and filtered through a 70 μm cell strainer, followed by erythrocyte lysis with ACK Lysing Buffer (Lonza; 10-548E). Bone marrow cells were plated in culture medium containing 20% conditioned L929 supernatant and medium was refreshed after 3 days and cells were used for experiments 6 days after isolation. BMDMs were cultured at 37°C and 5% CO_2 in RPMI 1640 medium supplemented with 10% FCS, 2mM glutamine (Lonza; BE17-605F), 1mM sodium pyruvate (Sigma-Aldrich; S8636), 100 U/ml penicillin, 100 μg/ml streptomycin (Sigma-Aldrich; P4333) and 20% conditioned L929 supernatant. Primary lung fibroblasts were isolated from lungs of 8-10-week-old male *Adar*$^{Z\alpha/Z\alpha}$ mice and wild-type littermates. Lungs were sterilized with 70% ethanol before cutting the tissue in pieces of ~25mm. Digestion was performed with a 0.1% collagenase D (Roche;11088866001) and 0.2% trypsin solution (GIBCO;15090-046) for 30 min at 37°C. The collagenase D / trypsin solution was refreshed and digestion continued another 30 minutes at 37°C. After neutralization with αMEM-20 [αMEM, GIBCO; 22571-020, supplemented with 20% FCS, 2mM glutamine (Lonza; BE17-605F), 1mM sodium pyruvate (Sigma-Aldrich; S8636), 100 U/ml penicillin and 100 μg/ml streptomycin (Sigma-Aldrich; P4333)], cells were pelleted at 400 g for 5 min and resuspended

in αMEM-20 culture medium. The purity of primary lung fibroblasts was assured by passaging each fibroblast line for at least 3 times in αMEM-20, which selectively supports growth of fibroblasts, whereas other cell types die or stop proliferating. Primary murine lung fibroblasts were maintained under hypoxic conditions (3% O_2 at 37°C and 5% CO_2 in αMEM-20).

METHOD DETAILS

Generation of *ADAR*$^{Z\alpha mut}$, *ADAR*$^{p150\text{-}KO}$, and *ADAR*^{KO} HEK293 clones

Cells were electroporated (NEPA21, NepaGene) with the indicated gRNAs and GFP-tagged Cas9 (VIB Protein Service Facility). *ADAR*^{KO} clones were generated using a gRNA#1 targeting against exon 2, which is shared by the ADAR1 p110 and p150 isoforms. The *ADAR*$^{p150\text{-}KO}$ clone was generated using gRNA#2 and gRNA#3 directed against exon 1A containing the p150-specific transcription start site. *ADAR*$^{Z\alpha mut}$ cells were generated by CRISPR/Cas9-mediated homology directed repair and using gRNA#4. A ssDNA repair template oligo containing the N173A/Y177A mutations was electroporated with the Cas9/gRNA complex. 24 hours after electroporation, single GFP-positive cells were FACS purified and plated into 96-well plates. Clones were screened by PCR and protein expression was analyzed by western blot. Zα domain mutation in *ADAR*$^{Z\alpha mut}$ clones was confirmed by Sanger sequencing and subcloning of the PCR fragments used for sequencing with the Zero Blunt TOPO PCR Cloning Kit (Invitrogen; 450245). At least 11 subclones were individually sequenced (see Figure S1A). Sequences of the gRNAs, ssDNA repair template and PCR primers are provided in Table S2.

Reagents

Mouse CXLC10 protein was quantified using ELISA (eBioscience; BMS6018MST) and Bio-Plex (Bio-Rad; #12002244). Human recombinant IFN-α2 was from Biolegend (592704) and hybrid IFNα-B/D was from Novartis (CGP35269).

Luciferase assays

HEK293 cells were seeded at a density of 200,000 cells per well of a 24-well plate and transfected 16 h later with 100 ng of the specified expression vectors (see Key Resources Table) using Lipofectamine 2000 (Invitrogen; 11668-027). For titration experiments, empty vector was added to the transfection mix to bring the total of input DNA to 200 ng. 50 ng of an IFN-β promoter reporter plasmid (p125-luc) and 20 ng of a *Renilla* luciferase reporter (pRL-TK; Promega E2241) under control of a thymidine kinase promoter were co-transfected. 24h after transfection, cells were washed with PBS and lysed in Passive Lysis Buffer, 5X (Promega; E194A). Luciferase units were measured by the Dual luciferase reporter assay system (Promega; E1910) on a Promega GloMax luminometer. Relative luciferase units (RLU) were calculated by dividing normalized luciferase units (Firefly / *Renilla*) by the normalized luciferase units from cells transfected with 200 ng empty vector for each HEK293 clone.

Western blotting and cellular fractioning

Fractioning of primary murine lung fibroblasts was performed with the Cell Fractionation Kit of Cell Signaling Technology (#9038S). For western blotting, cells were washed with ice-cold PBS and lysed in protein lysis buffer (50mM Tris HCl, pH 7.5, 1% Igepal CA-630 and 150mM NaCl) supplemented with complete protease inhibitor cocktail (Roche; 11697498001) and PhosSTOP (Roche;4906845001). Lysates were cleared by centrifugation at 12,000 g for 15 min and 5x Laemlli loading buffer (250mM Tris HCl, pH 6.8, 10% SDS, 0.5% Bromophenol Blue, 50% glycerol and 20% β-mercaptoethanol) was added to the supernatant. Finally, samples were incubated at 95°C for 5 min and analyzed using Tris-Glycine SDS-PAGE and semi-dry immunoblotting. Primary and secondary antibodies for western blotting are listed in the Key Resources Table.

qRT-PCR

Tissue sections were homogenized with the Precellys 24 Tissue Homogenizer and 1.4 mm Zirconium oxide beads (VWR International; P000927-LYSK0-A) in Trizol reagent (GIBCO BRL; 15596-018). For both tissues and cells, total RNA was purified using RNeasy colums (QIAGEN) with on-column DNase I digestion. cDNA synthesis was performed with the SensiFast cDNA synthesis kit (Bioline; BIO-65054). SensiFast SYBR No-Rox kit (Bioline; BIO-98005) or PrimeTime qPCR Master Mix (IDT; 1055771) was used for cDNA amplification using a Lightcycler 480 system (Roche). Primers and probes are listed in Table S2.

Tissue and peripheral blood processing for flow cytometry

Lungs and spleens of 8-10 week old *Adar*$^{Z\alpha/Z\alpha}$ and wild-type littermates were collected in ice-cold PBS. Lungs were processed according to (Fletcher et al., 2011) with minor modifications. In brief, lungs were digested for 1 hour at 37°C in digestion buffer [RPMI 1640 supplemented with 10% FCS, 0.8 mg/ml dispase II (Invitrogen; 17105-041), 0.2 mg/ml collagenase P (Sigma-Aldrich; 000000011213857001) and 0.1% DNase I (Roche; 1010459001)] with regular mixing. After neutralisation with FACS buffer without sodium azide (PBS, 5% FCS, 1 mM EDTA), erythrocytes were lysed with ACK Lysing Buffer (Lonza; 10-548E) and filtered through a 100 μm cell strainer to obtain single cell solutions. Next, cells were stained with anti-mouse CD16/CD32 (Fc-block; BD Biosciences; 553142) and anti-mouse CD45-FITC before magnetic separation using anti-FITC microbeads (Miltenyi Biotec; 130-048-701) on midiMacs type LS separation columns (Miltenyi Biotec; 130-042-401). Spleens were digested for 30 min at 37°C in digestion buffer [(RPMI 1640 supplemented 0.5 mg/ml collagenase D (Roche; 11088866001) and 10 μg/ml DNase I (Roche; 1010459001)] with regular mixing.

After neutralisation with RPMI 1640 medium containing 2% FCS, erythrocytes were lysed with ACK Lysing Buffer (Lonza; 10-548E) and filtered through a 70 μm cell strainer to obtain single cell solutions. Peripheral blood was collected in EDTA-coated tubes (Sarstedt; 20.1288) by tail vein bleeding. 1 mL ACK Lysing Buffer (Lonza; 10-548E) was mixed with 100 μl blood and incubated for 10 min at RT. Cells were washed 2 times with ice-cold PBS and were stained for flow cytometry analysis.

Flow cytometry

Single cell suspensions were first stained with anti-mouse CD16/CD32 (Fc-block; BD Biosciences; 553142) and dead cells were excluded with the Fixable Viability Dye eFluor506 (eBioscience; 65-0866-14) for 30 min at 4°C in PBS. Next, cell surface markers were stained for 30 min at 4°C in FACS buffer (PBS, 5% FCS, 1mM EDTA and 0.05% sodium azide). Cells were acquired on an LSR Fortessa or a FACSymphony (BD Biosciences) or sorted on a Aria III sorter (BD Biosciences). Data were analyzed with FlowJo software (Tree Star). The total number of cells was counted on a FACSVerse (BD Biosciences). Fluorochrome-conjugated antibodies are listed in the Key Resources Table.

Blood analysis

Peripheral blood was collected in EDTA-coated tubes by tail vein bleeding. Total number of leukocytes, erythrocytes whole-blood parameters were determined using a HEMAVET950LV (Drew Scientific).

RNA-seq library preparation

Total RNA of IFN-α2 treated HEK293 cells was purified using RNeasy columns (QIAGEN) with on-column DNase I digestion. RNA integrity was tested with the Agilent RNA 6000 Pico Kit (Agilent; 50671513). Sequencing libraries were prepared using the Truseq Stranded Total RNA kit (Illumina) with the Ribo-Zero Gold kit (Illumina) for ribosomal depletion. Total RNA of primary murine lung endothelial cells was purified using RNeasy Micro columns (QIAGEN) with on-column DNase I digestion. RNA integrity was checked with the Agilent RNA 6000 Pico Kit (Agilent; 50671513). Libraries were prepared using the SMARTseq Stranded Total RNA kit (Takara Bio) with ZapR kit (Takara Bio) for ribosomal depletion. Libraries were sequenced on an Illumina HiSeq3000 genreating 150 bp paired-end sequencing reads.

Differential gene expression analysis

Quality control of raw Fastq files was performed with FastQC v0.11.7. Trimmomatic v1.4 was used for clipping of adaptor and index sequences with default parameters. Paired-end reads were mapped to the murine reference genome (GRCm38) using STAR 2.7.3a in 2-pass mode. Raw read counts were determined using HTSeq 0.11.1 in union mode. Normalized counts were calculated with R-package DESeq2 (v1.26.0). Gene ontology enrichment was analyzed using DAVID (https://david.ncifcrf.gov/); functional annotation; ENSEMBLE_GENE_ID; GO-term BP direct; Bonferonni EASE = 0.05.

A-to-I editing analysis

In addition to adaptor and index sequence clipping, Trimmomatic v1.4 was used to crop the first 15 bp and last 6 bp of the reads to circumvent bias introduced by random priming. Trimmed paired-end reads were mapped to the reference genome (HEK293; assembly hg19, murine lung endothelial cells; assembly mm10) using STAR 2.7.3a. Obtained BAM files (sorted by coordinate), the reference genome and machine learning training sets functioned as input files for the RDDpred tool (v1.1) (Kim et al., 2016). RDDpred was used for the detection of RNA-DNA differences. Training sets consisted of Mapping Error-prone Sites (negative set; http://epigenomics.snu.ac.kr/RDDpred/prior.php) and annotated A-to-I editing sites (positive set) derived from the DARNED (Kiran et al., 2013), RADAR (Ramaswami and Li, 2014) and REDIportal (Mansi et al., 2021) databases. Murine editing sites derived from the RADAR database were converted from mm9 to mm10 assembly using LiftOver (Kuhn et al., 2013). To assign strand topology to each identified RNA-DNA difference (RDD), BAM files were split in half-samples containing reads that were either mapped to the sense or antisense strand. Bam-readcount (https://github.com/genome/bam-readcount) was used to determine read coverage and variant frequency for all RDDs in each half-sample. Ambiguous RDDs (e.g., multiple variant calls per site, RDD detected on both strands), were excluded from downstream analysis. In addition, sites overlapping with annotated C57BL/6-specific SNPs extracted from the Sanger Institute Mouse Genomes project v3 (dbSNPv137) and sites overlapping annotated SNPs were removed from further downstream analysis. HEK293-specific SNPs were retrieved from http://hek293genome.org/v2/data.php; data track CG 293 and converted to hg19 assembly using LiftOver. For HEK293 samples, an additional filtering step based on RDDs that were also detected in the ADAR1 KO sample was performed. Genomic annotation of the identified A-to-I editing sites was assigned using GENCODE basic annotation (HEK293; release 34, mouse: release 25, hierarchy: 3′ UTR > 5′ UTR > Exon > Intron > Intergenic > Downstream > Promoter) and repeat element status was determined based on RepeatMasker annotation (www.repeatmasker.org; Repeat Library 20140131). For differential editing analysis, the editing index was calculated (variant count / total count) and sites with a read count below 10 or editing index of 0 were discarded. Differentially edited sites (p value < 0.05) were determined by the Welch Two Sample t test log10 values of the calculated editing index.

QUANTIFICATION AND STATISTICAL ANALYSIS

Statistical analyses were performed using Prism 8.2.1 (GraphPad Software). Statistical methods are described in the figure legends.

Cell Reports, Volume *36*

Supplemental information

ADAR1 interaction with Z-RNA promotes editing of endogenous double-stranded RNA and prevents MDA5-dependent immune activation

Richard de Reuver, Evelien Dierick, Bartosz Wiernicki, Katrien Staes, Leen Seys, Ellen De Meester, Tuur Muyldermans, Alexander Botzki, Bart N. Lambrecht, Filip Van Nieuwerburgh, Peter Vandenabeele, and Jonathan Maelfait

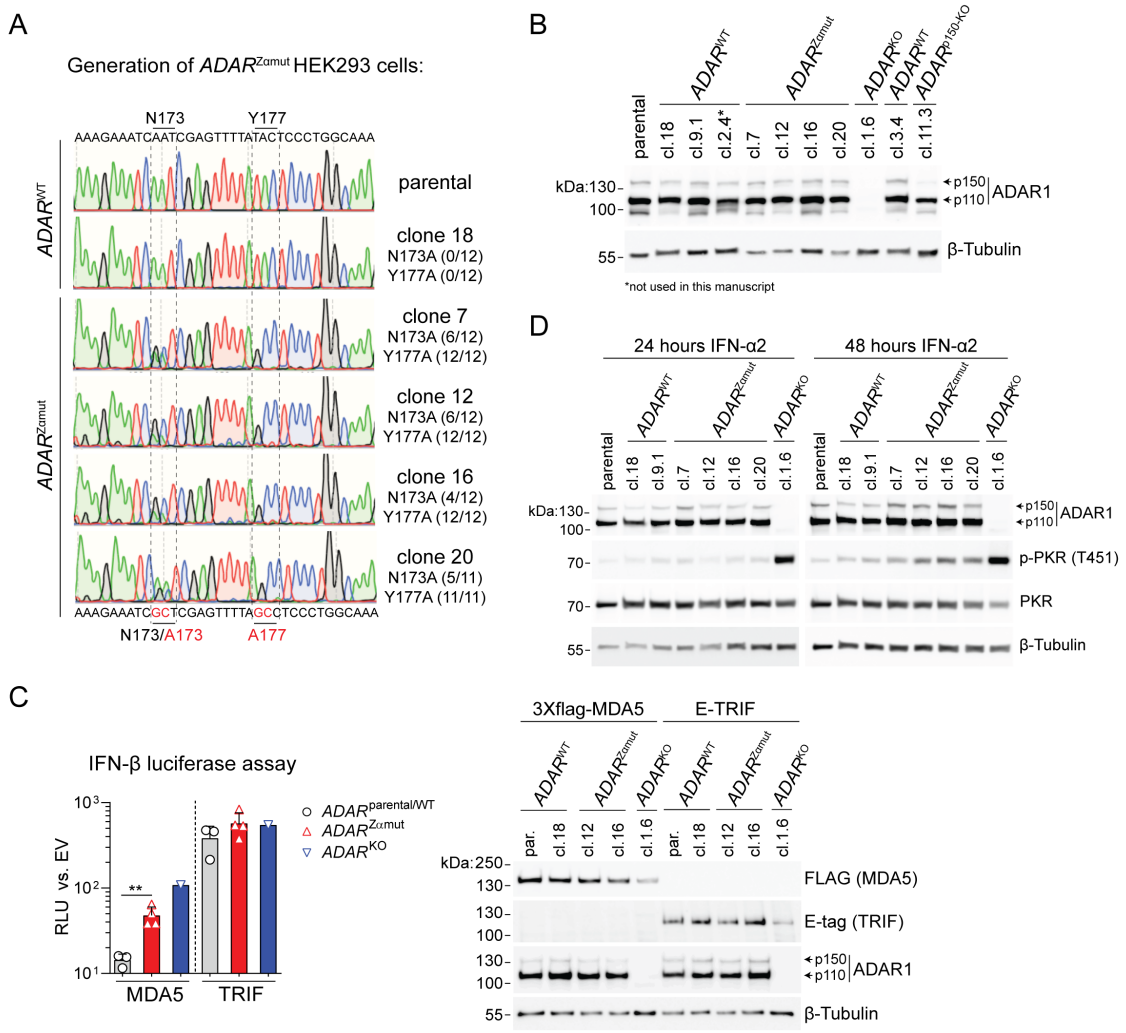

Figure S1. ADAR1 Zα-domain mutation activates MDA5 in human cells, Related to Figure 1.
(A) Sanger sequencing profiles of the parental HEK293 cells and ADAR1 wild type (*ADAR*^{WT}) and Zα-domain mutant (*ADAR*^{Zαmut}) HEK293 clones. Ratios indicate the frequency of wild type (N173/Y177) or mutant (A173/A177) alleles determined by Sanger sequencing of 11 or 12 PCR subclones.
(B) HEK293 clones of the indicated genotypes were stimulated for 24 h with 1000 U/ml IFN-α2. Protein expression of ADAR1 was analysed by Western blotting. Arrows indicate the ADAR1 p110 and p150 isoform.
(C) Parental HEK293 cells, *ADAR*^{WT}, *ADAR*^{Zαmut} or ADAR1-deficient (*ADAR*^{KO}) clones were transfected with 50 ng IFN-β promoter firefly luciferase and 20 ng *Renilla* luciferase reporter plasmids, together with FLAG-tagged human MDA5 or E-tagged human TRIF. Luciferase activity was analysed as in Figure 1B. Protein expression of ADAR1, FLAG-tagged MDA5 and E-tagged TRIF was verified by Western blot (right panel). Arrows indicate the ADAR1 p110 and p150 isoform. **, $P < 0.01$ by unpaired t-test.
(D) HEK293 clones of the indicated genotypes were stimulated for 24 or 48 h with 1000 U/ml IFN-α2. Protein expression of ADAR1, threonine 451 (T451) phosphorylated PKR (p-PKR) and total PKR was analysed by Western blotting. Arrows indicate the ADAR1 p110 and p150 isoform. Data in (C) and (D) are representative of at least two independent experiments.

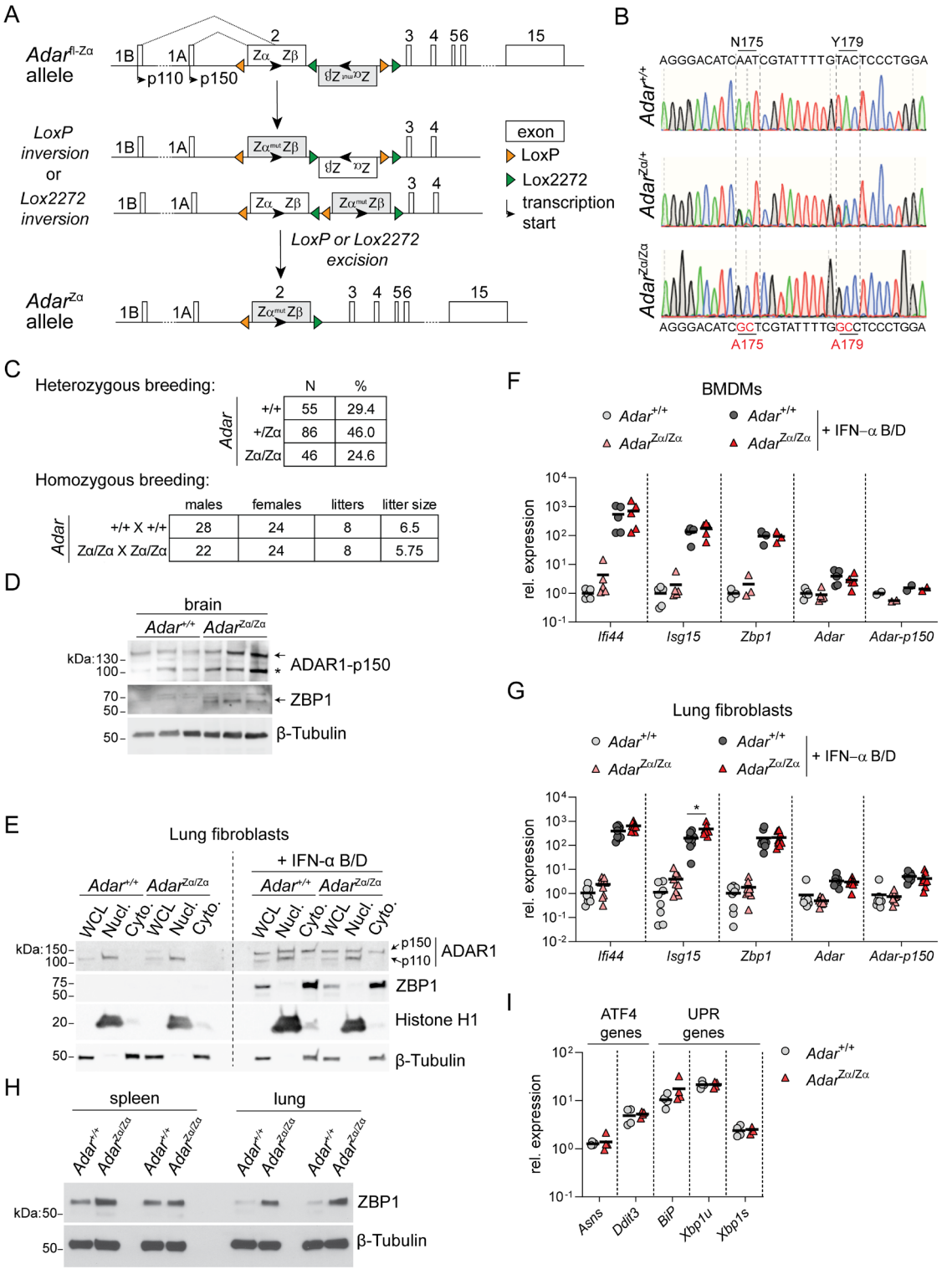

Figure S2. *Adar* Zα-domain mutant mice develop a spontaneous antiviral immune response, Related to Figure 2.

(A) Schematic overview of the strategy to create the conditional ADAR1 N175A/Y179A Zα-domain knock-in (*Adar*$^{fl\text{-}Z\alpha}$) mice.

(B) Sanger sequencing chromatograms of *Adar*$^{+/+}$, *Adar*$^{+/Z\alpha}$ and *Adar*$^{Z\alpha/Z\alpha}$ mice.

(C) Overview of the offspring obtained from both heterozygous (*Adar*$^{+/Z\alpha}$ X Adar$^{+/Z\alpha}$) and homozygous (*Adar*$^{Z\alpha/Z\alpha}$ X *Adar*$^{Z\alpha/Z\alpha}$) breeding pairs.

(D) Protein expression of ADAR1-p150, ZBP1 and β-tubulin in brain extracts was analysed by Western blot. The arrows indicate ADAR1-p150 or ZBP1 and * a non-specific band.
(E) Primary lung fibroblasts from *Adar*$^{+/+}$ and *Adar*$^{Zα/Zα}$ mice were left untreated or stimulated for 18 hours with 200 U/ml IFN-α B/D. Protein samples were fractioned into whole-cell lysates (WCL), nuclear (Nucl.) or cytosolic (Cyto.) lysates. Protein expression of ADAR1 (isoform p110 and p150), ZBP1, Histone H1 and β-tubulin were analysed by Western blot.
(F-G) RT-qPCR analysis of the indicated ISGs in BMDMs (F) and primary lung fibroblasts (G) from *Adar*$^{+/+}$ and *Adar*$^{Zα/Zα}$ mice left untreated or stimulated for 18 hours with 200 U/ml IFN-α B/D. Data are pooled from two independent experiments. The mean relative expression of each gene in untreated *Adar*$^{+/+}$ fibroblasts is set at 1. *, $P < 0.05$ by unpaired t-test.
(H) Protein samples were prepared from spleens and lungs of 2 individual *Adar*$^{+/+}$ and Adar$^{Zα/Zα}$ mice. Protein expression of the ISG ZBP1 was analysed by Western blot.
(I) RT-qPCR analysis of *Asns*, *Ddit3*, *BiP* (or *Hspa5*) and *Xbp1* in the unspliced (*Xbp1u*) and spliced (*Xbp1s*) form in the lungs of *Adar*$^{+/+}$ and Adar$^{Zα/Zα}$ mice.

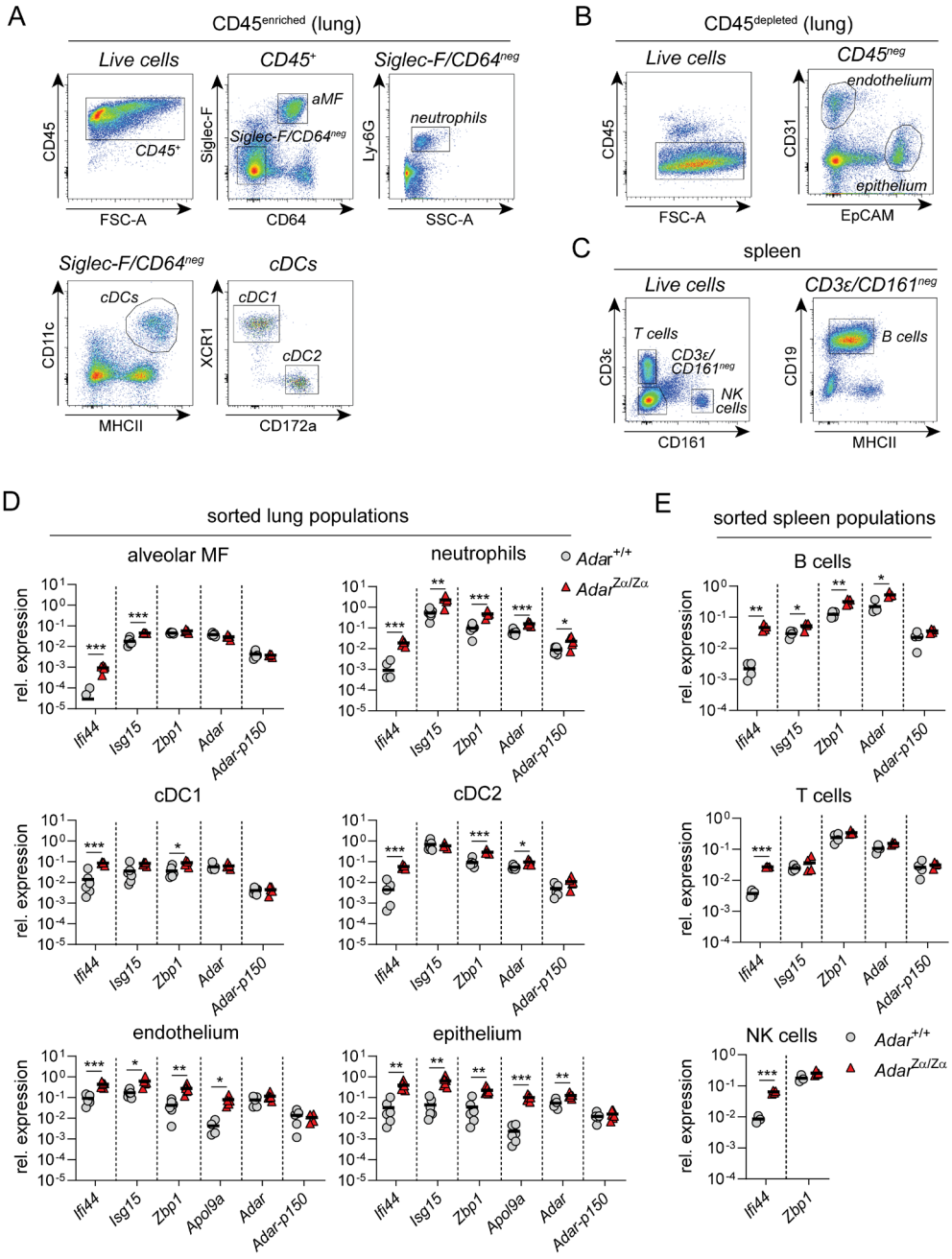

Figure S3. Characterisation of ISG expression in lung and spleen cell types of *Adar*$^{Zα/Zα}$ mice, Related to Figure 2.

(A and B) Gating strategy for FACS purification of CD45^{+} leukocytes (A) including alveolar macrophages, neutrophils, conventional type 1 and type 2 dendritic cells (cDC1 and cDC2) and CD45^{-} (B) endothelial and epithelial cells from lungs of *Adar*$^{Zα/Zα}$ mice and control littermates.

(C) Gating strategy for FACS purification of B cells, T cells and NK cells from the spleens of *Adar*$^{+/+}$ and *Adar*$^{Zα/Zα}$ mice.

(D and E) RT-qPCR analysis of the indicated ISGs in the indicated cell populations derived from the lungs (D) and spleens (E) of *Adar*$^{+/+}$ and *Adar*$^{Zα/Zα}$ mice. *, $P < 0.05$, **, $P < 0.01$, ***, $P < 0.001$ by unpaired t-test. Each data point in (D) and (E) represents an individual mouse. Lines indicate the mean. Data in (D) are representative of at least 2 independent experiments.

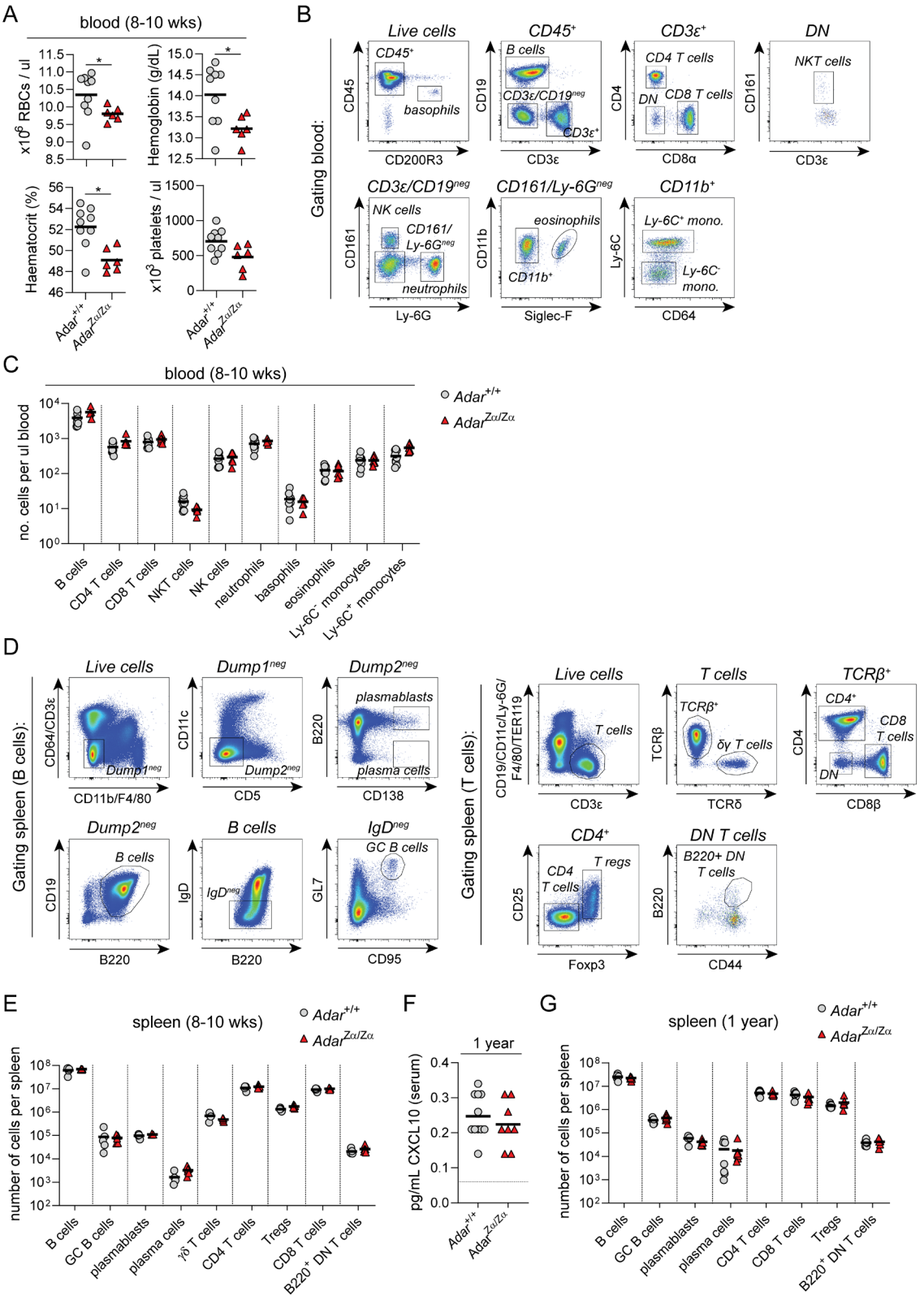

Figure S4. *Adar*$^{Zα/Zα}$ mice maintain normal haematopoiesis and do not develop autoinflammatory disease, Related to Figure 4.

(A) Peripheral blood from 8-10 week old *Adar*$^{Zα/Zα}$ mice and their wild-type littermates (*Adar*$^{+/+}$) was analysed for total red blood cell and platelets numbers and haematocrit and haemoglobin levels. *, P < 0.05 by Mann–Whitney U test.

(B and C) Gating strategy (B) used for flow cytometry analysis of circulating lymphocytes (B cells, CD4 and CD8 T cells, and NK and NKT cells) or myeloid cells (neutrophils, basophils, eosinophils, and Ly-6C^{-} and Ly-6C^{+} monocytes) (C).
(D, E and G) Gating strategy (D) used for flow cytometry analysis of the splenic T and B cell compartment of 8-10 week (E) and 1 year (G) old *Adar*$^{+/+}$ and *Adar*$^{Zα/Zα}$ mice.
(F) Analysis of CXCL10 protein levels in serum of 1 year old *Adar*$^{+/+}$ and *Adar*$^{Zα/Zα}$ mice by Bio-Plex assay.
Each data point in (A), (C), (E-G) represents an individual mouse. Lines indicate the mean.

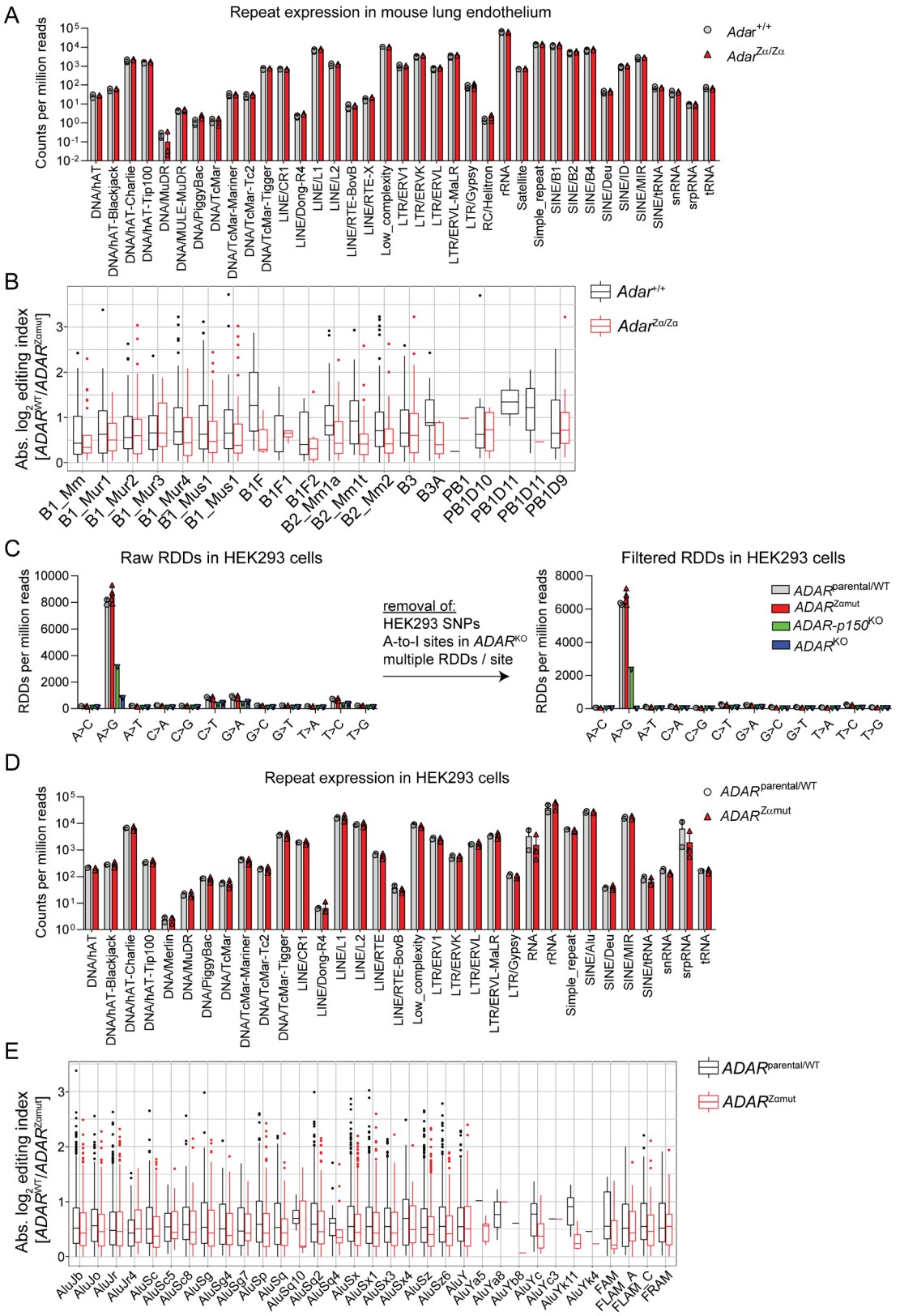

Figure S5. Loss of ADAR1/Z-RNA interaction results in reduced A-to-I editing of SINEs, Related to Figure 5.

(A) Expression levels in counts per million reads of repetitive elements in lung endothelial cells of *Adar*$^{+/+}$ and *Adar*$^{Zα/Zα}$ mice

(B) Box plot showing differential A-to-I editing of members of the mouse SINE B1 and B2 families in lung endothelial cells of *Adar*$^{+/+}$ and *Adar*$^{Z\alpha/Z\alpha}$ mice calculated using the same approach as in Figure 5 (C) and (D).
(C) Bar charts displaying RNA-DNA differences (RDDs) per million reads in parental HEK293 cells, wild type (*ADAR*^{WT}), Zα-domain mutant (*ADAR*$^{Z\alpha mut}$), ADAR1-p150 deficient (*ADAR-p150*^{KO}) and ADAR1-deficient (*ADAR*^{KO}) HEK293 clones. Left panel: raw RDDs discovered after RDDpred and BAMreadcount. Right panel: refined dataset after removing sites containing multiple RDDs, A>G mismatches discovered in the *ADAR*^{KO} clones and HEK293-specific SNPs.
(D) Expression levels in counts per million reads of repetitive elements in HEK293 cells of the indicated genotype.
(E) Box plot showing differential A-to-I editing of members of the human SINE Alu family in *ADAR* wild type (*ADAR*$^{parental/WT}$) and Zα-domain mutant (*ADAR*$^{Z\alpha mut}$) HEK293 cells calculated using the same approach as in Figure 5 (C) and (D).

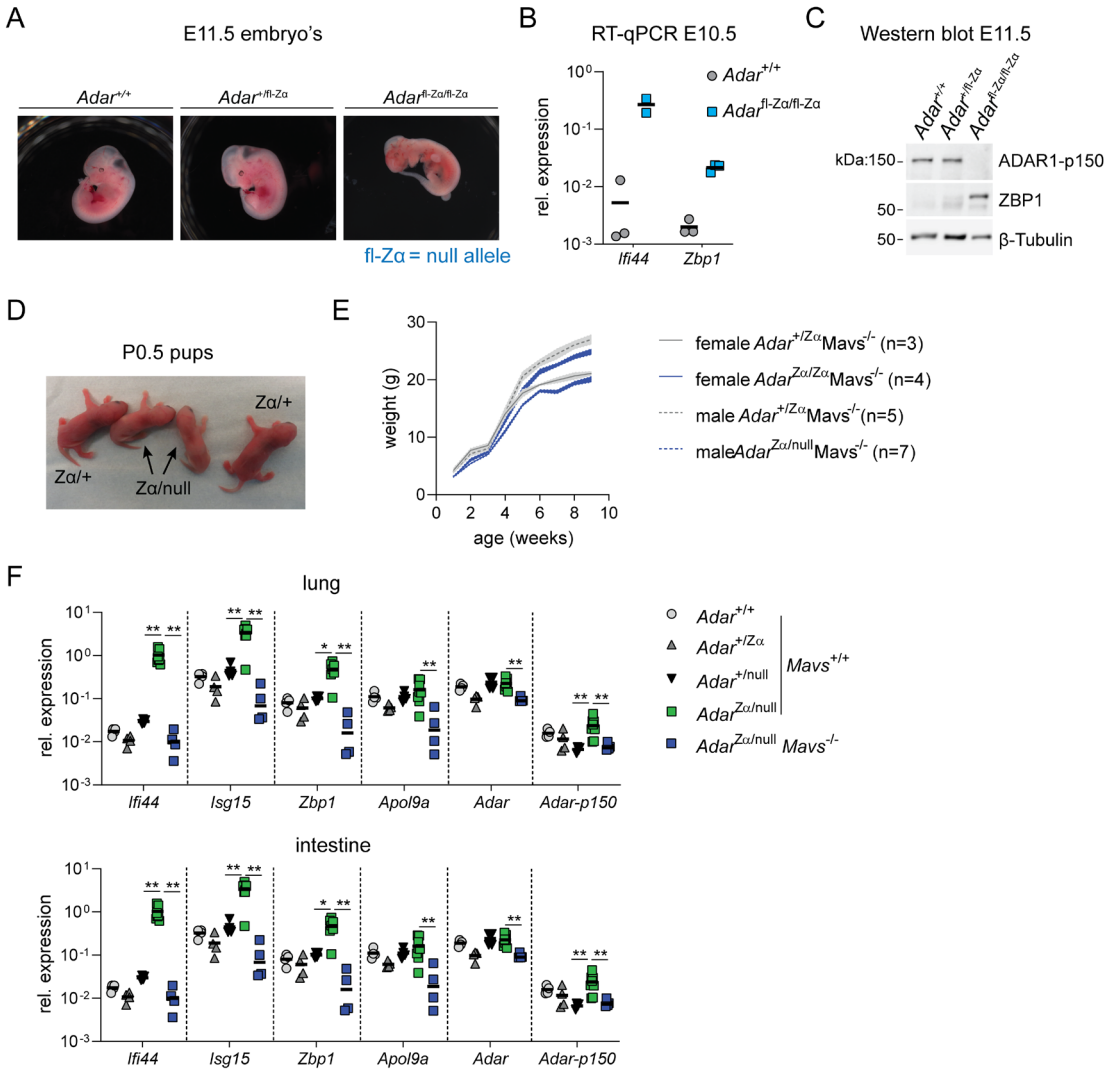

Figure S6. Compound heterozygous *Adar*$^{Zα/null}$ mice die postnatally and develop a severe MAVS-dependent IFN-I response, Related to Figure 6.

(A) Macroscope pictures of embryonic day (E) 11.5 *Adar*$^{+/+}$, *Adar*$^{+/fl\text{-}Zα}$ and *Adar*$^{fl\text{-}Zα/fl\text{-}Zα}$ embryos.

(B) RT-qPCR analysis of *Ifi44* and *Zbp1* on RNA extracted from E10.5 embryos of the indicated genotypes.

(C) Protein expression of ADAR1-p150, ZBP1, and β-tubulin in whole embryo extracts from the indicated genotypes was analysed by Western blot.

(D) Picture of newborn *Adar*$^{Zα/null}$ pups and control *Adar*$^{Zα/+}$ littermates at postnatal day 0.5 (P0.5).

(E) Weight in grams (g) of male and female mice of the indicated genotype was measured weekly from 1 until 9 weeks of age. Lines represent mean and shaded area shows ± SEM**.**

(F) RT-qPCR analysis of the indicated ISGs in lung and intestine from P0.5 mice of the indicated genotypes. Lines represents the mean, and symbols depict individual mice. *, P < 0.05, **, P < 0.01 by unpaired t-test.